AMERICAN SOCIETY FOR MICROBIOLOGY | Applied and Environmental Microbiology

Spotlight Selection | Systems Biology | Full-Length Text

Mechanistic insights into sulfur source-driven physiological responses and metabolic reorganization in the fuel-biodesulfurizing *Rhodococcus qingshengii* IGTS8

Julie Zumsteg,[1] Aurélie Hirschler,[2] Christine Carapito,[2] Loïc Maurer,[1,3] Claire Villette,[1] Dimitri Heintz,[1] Christiane Dahl,[4] Ashraf El Nayal,[5] Vartul Sangal,[6] Huda Mahmoud,[7] Alain Van Dorsselaer,[2] Wael Ismail[5]

AUTHOR AFFILIATIONS See affiliation list on p. 24.

ABSTRACT Comparative proteomics and untargeted metabolomics were combined to study the physiological and metabolic adaptations of *Rhodococcus qingshengii* IGTS8 under biodesulfurization conditions. After growth in a chemically defined medium with either dibenzothiophene (DBT) or $MgSO_4$ as the sulfur source, many differentially produced proteins and metabolites associated with several metabolic and physiological processes were detected including the metabolism of carbohydrates, amino acids, lipids, nucleotides, vitamins, protein synthesis, transcriptional regulation, cell envelope biogenesis, and cell division. Increased production of the redox cofactor mycofactocin and associated proteins was one of the most striking adaptations under biodesulfurization conditions. While most central metabolic enzymes were less abundant in the presence of DBT, a key enzyme of the glyoxylate shunt, isocitrate lyase, was up to 26-fold more abundant. Several C1 metabolism and oligotrophy-related enzymes were significantly more abundant in the biodesulfurizing culture. *R. qingshengii* IGTS8 exhibited oligotrophic growth in liquid and solid media under carbon starvation. Moreover, the oligotrophic growth was faster on the solid medium in the presence of DBT compared to $MgSO_4$ cultures. In the DBT culture, the cell envelope and phospholipids were remodeled, with lower levels of phosphatidylethanolamine and unsaturated and short-chain fatty acids being the most prominent changes. Biodesulfurization increased the biosynthesis of osmoprotectants (ectoine and mannosylglycerate) as well as glutamate and induced the stringent response. Our findings reveal highly diverse and overlapping stress responses that could protect the biodesulfurizing culture not only from the associated sulfate limitation but also from chemical, oxidative, and osmotic stress, allowing efficient resource management.

IMPORTANCE Despite decades of research, a commercially viable bioprocess for fuel desulfurization has not been developed yet. This is mainly due to lack of knowledge of the physiology and metabolism of fuel-biodesulfurizing bacteria. Being a stressful condition, biodesulfurization could provoke several stress responses that are not understood. This is particularly important because a thorough understanding of the microbial stress response is essential for the development of environmentally friendly and industrially efficient microbial biocatalysts. Our comparative systems biology studies provide a mechanistic understanding of the biology of biodesulfurization, which is crucial for informed developments through the rational design of recombinant biodesulfurizers and optimization of the bioprocess conditions. Our findings enhance the understanding of the physiology, metabolism, and stress response not only in biodesulfurizing bacteria but also in rhodococci, a precious group of biotechnologically important bacteria.

Editor Marina Lotti, University of Milano-Bicocca, Milan, Italy

Address correspondence to Wael Ismail, waelame@agu.edu.bh.

The authors declare no conflict of interest.

See the funding table on p. 25.

Received 23 May 2023
Accepted 30 June 2023
Published 1 September 2023

KEYWORDS mycofactocin, metabolomics, stress response, *Rhodococcus*, comparative proteomics, lipid metabolism, oligotrophy

Microbial biodesulfurization emerged as a green process for removing sulfur from fossil fuels (1–3) to meet environmental regulations and satisfy the ever-increasing global demand for cleaner fuels (4–6). Fuel biodesulfurization is based on the unique metabolic capability of some bacteria to utilize sulfur-containing compounds (such as dibenzothiophene, DBT) found in diesel fuel as their sole sulfur source without consuming the carbon skeleton of these compounds. This is achieved via the sulfur-specific 4S pathway discovered in the biodesulfurization model organism *Rhodococcus qingshengii* IGTS8 (1–3, 7). Over the past three decades, several attempts have been made to increase the biodesulfurization catalytic activity via genetic engineering and physicochemical strategies that have been implemented to enhance the biodesulfurization activity of different bacteria (8–14). Despite these enormous efforts, a process for the biological desulfurization of fossil fuels has not yet been commercialized, in part due to the very low catalytic activity and insufficient robustness of the biocatalysts/microbial hosts used (11, 15). Furthermore, the almost exclusive focus on the 4S pathway has left large gaps in our understanding of the general physiological and metabolic adaptations of biodesulfurizing microbes, which is essential for the development of efficient desulfurization bioprocesses (11, 15–19).

In fact, there is accumulating evidence that other metabolic features besides the 4S pathway are critical for the biodesulfurization phenotype (4). For example, different bacteria harboring identical genes for the 4S pathway enzymes exhibit different biodesulfurization phenotypes (4, 20, 21). On the other hand, Tanaka et al. (22) found that the biodesulfurization activity of *Rhodococcus erythropolis* KA2-5-1 was stimulated in the presence of the biodesulfurization-inhibiting inorganic sulfate by disruption of the gene-encoding cystathionine β-synthase, an enzyme involved in sulfur assimilation. Based on a genome-scale metabolic model, Aggarwal et al. (16) suggested that a simultaneous decrease in sulfite reductase activity and an increase in sulfite oxidoreductase activity improve the biodesulfurization rate via the 4S pathway. Dorado-Morales et al. (23) improved the biodesulfurization activity by inducing biofilm formation in *R. erythropolis*.

These findings have highlighted the need for systematic in-depth studies to better understand the physiology and metabolism of biodesulfurizing bacteria and to identify genetic/metabolic engineering hotspots for the development of more catalytically efficient biodesulfurizers. While comparative systems biology approaches have been widely applied to understand the metabolic and physiological responses of bacteria to different stresses (24–27), only a few studies exist for fuel-biodesulfurizing bacteria (28, 29). To fill this gap, we performed comparative proteomics and metabolomics on the biodesulfurization model organism *R. qingshengii* IGTS8 grown on either $MgSO_4$ or the diesel-borne organosulfur compound DBT as the main sulfur source (19). Since DBT is an unconventional sulfur source (less preferred than inorganic sulfate) (30), we hypothesized that under biodesulfurization conditions, *R. qingshengii* IGTS8 undergoes metabolic and physiological adaptations that are reflected in the proteome and metabolome. Indeed, we found significant biodesulfurization-related and growth phase-dependent shifts in the abundance of sulfur assimilation proteins and metabolites (19). Further adaptations concerned the biosynthesis of key sulfur-containing metabolites such as *S*-adenosylmethionine, coenzyme A, biotin, thiamin, the molybdenum cofactor, and the low-molecular-weight thiols mycothiol and ergothioneine. Based on these data, we developed a model for sulfur assimilation during biodesulfurization (19). In another recent study on *R. qingshengii* IGTS8, Martzoukou et al. (31) showed that typical sulfur assimilation enzymes, namely cystathionine β-synthase and cystathionine γ-lyase, play a role in sulfate- and methionine-dependent repression of the 4S biodesulfurization pathway enzymes.

Here, we further explored our proteomics and metabolomics data, conducted genomic analyses, and found significant global differences between sulfate-assimilating and biodesulfurizing *R. qingshengii* IGTS8 cells. These data indicate that the response reaches far beyond sulfur assimilation and further confirms the importance of a thorough understanding of the physiology and metabolism of biodesulfurizing bacteria.

MATERIALS AND METHODS

Composition of the chemically defined medium

Chemically defined medium (CDM) was prepared in deionized water with the following composition per liter: KH_2PO_4, 1.08 g; K_2HPO_4, 5.6 g; NH_4Cl, 0.54 g; $CaCl_2.2H_2O$, 0.044 g; $FeCl_2.4H_2O$, 1.5 mg; vitamins (cyanocobalamine 0.2 mg, pyridoxine-HCl 0.6 mg, thiamin-HCl 0.4 mg, nicotinic acid 0.4 mg, *p*-aminobenzoate 0.32 mg, biotin 0.04 mg, Ca-pantothenate 0.4 mg); and trace elements ($ZnCl_2.7H_2O$: 70 µg, $MnCl_2.4H_2O$: 100 µg, $CuCl_2$: 20 µg, $CoCl_2.6H_2O$: 200 µg, $Na_2MoO_4.2H_2O$: 40 µg, $NiCl_2.6H_2O$: 20 µg, H_3BO_3: 20 µg). In the inorganic sulfate cultures, $MgSO_4.7H_2O$ (0.5 mM) was added as the main sulfur source, while the biodesulfurizing cultures had DBT (0.5 mM) (added from a 100-mM stock in ethanol) as the main sulfur source. In addition, $MgCl_2.6H_2O$ (0.5 mM) was added to the DBT cultures to compensate for the Mg concentration. No $MgCl_2$ was added to the inorganic sulfate cultures. The carbon source (glucose) was added at a concentration of 20 mM in both cultures. In addition, the biodesulfurizing culture had ethanol (0.5%, vol/vol) as the co-solvent of DBT.

Culturing of *R. qingshengii* IGTS8

Comparative proteomics and untargeted metabolomics on *R. qingshengii* IGTS8 (ATCC 53968) were conducted as described by Hirschler et al. (19). The strain IGTS8 was grown in CDM with either $MgSO_4$ or DBT as the main sulfur source, and glucose or glucose + ethanol as the carbon source, respectively (19). Four biological replicates were prepared for each culture, and there was a separate set of cultures for each harvesting time point, that is, there was a total number of 16 cultures for each sulfur source (four time points × four replicates). For the DBT cultures, cells were harvested after 32 hours (early-log phase), 45.5 hours (mid-log phase), 54.5 hours (late-log phase), and 67.5 hours (stationary phase). For the inorganic sulfate-containing cultures, cells were harvested after 29 hours (early-log phase), 36 hours (mid-log phase), 41 hours (late-log phase), and 45.5 hours (stationary phase). Growth curves of both cultures are included in Fig. S1.

Quantitative proteomics

Details of sample preparation and nano liquid chromatography coupled to tandem mass spectrometry (LC-MS/MS) analysis are included in the Supplementary Material and described in Hirschler et al. (19). Raw MS data were processed using MaxQuant software v1.6.0.16 (32). Peak lists were searched against the *R. qingshengii* IGTS8 proteins (6,734 sequences). The annotated genome is accessible via FigShare (DOI: https://dx.doi.org/10.6084/m9.figshare.14547426). MaxQuant parameters were set as follows: MS tolerance set to 20 ppm for the first search and 5 ppm for the main search, MS/MS tolerance set to 40 ppm, maximum number of missed cleavages set to 2, Carbamidomethyl (C) set as a fixed modification, Oxidation (M), and Acetylation (Protein N-term) set as variable modifications. Identifications were validated at a false discovery rate (FDR) below 1% at both peptide spectrum match and protein levels. Data normalization and protein quantification were performed using label-free quantification (LFQ) with a "minimal ratio count" of one. The "Match between runs" option was enabled using a 2-minute time window after retention time alignment. All other MaxQuant parameters were set as default. Differential data analysis was performed using the open-source ProStaR software version 1.24.7 (33). To be considered for differential analysis, proteins must be identified in all four replicates of the DBT or MgSO4 cultures. For residual missing

values, the slsa algorithm was used for the POV (Partially Observed Values) imputation, and MEC (Missing on the Entire Condition) values were replaced by the 2.5 percentile value. A Limma moderated *t*-test was applied to the data set to perform differential analysis. Benjamini-Hochberg method was used to adjust *P*-values for multiple testing, and differentially expressed proteins were sorted out using a *P*-value threshold that guarantees an FDR below 1%. Complete data set has been deposited to the ProteomeXchange Consortium via the PRIDE partner repository (34) with the data set identifier PXD021362. Data were analyzed with principal component analysis (PCA) on R (version 3.6.3) using the MetaboAnalyst package. The PCA test was built considering the different proteins as individuals and the growth phases as variables. The PCA results indicate that the two first axis represent 70.4% of the data set inertia (variability of the data cloud).

Functional classification of the detected proteins

To perform functional classification of the differentially expressed proteins, a BLAST fasta36 search was performed (35). Similarity search was done against a public *Rhodococcus qingshengii* genome from UniProtKB/Swiss-Prot (TaxID 334542, 16,072 entries, 24 November 2021). For each protein, gene ontology (GO) terms were queried from the Gene Ontology database (http://geneontology.org/) and proteins were filtered according to their functional classification.

Enrichment analysis of the differential proteins

Functional annotation enrichment analysis of differential proteomics data was performed for each growth phase in an unbiased way using the desktop version of DAVID (Ease v2.0) (36, 37) and an updated version of GO and KEGG pathway databases (18 October 2021). The list of differentially produced proteins from each comparison (DBT and $MgSO_4$ cultures) was compared to the list of all proteins identified. Enriched GO terms were filtered by only considering those with an Ease score lower than 0.1 and a Benjamini *P*-value < 0.05.

Metabolomics analyses

Sample preparation procedures and untargeted LC-MS/MS analysis are described in detail in the Supplementary Material and Hirschler et al. (19).

Untargeted gas chromatography-mass spectrometry (GC-MS) analysis

Fifty microliters of each extract were dried in a SpeedVac (Thermo Scientific) and derivatized by adding 50 µL of a solution of methoxyamine hydrochloride (Sigma), pyridine (>99.5%, Sigma), and a mixture of nine alkanes (C10-C12-C15-C18-C19-C22-C28-C32-C36 used as internal standards). The samples were heated at 40°C for 90 minutes and shaken at 900 rpm in a thermomixer. Eighty microliters of *N*,*O* bis(trimethylsilyl)trifluoroacetamide (>99%, Sigma) were added, and the microtubes were heated for 30 minutes at 40°C at 900 rpm. We used two different methods to analyze the extracts. Silylated samples were analyzed by GC (436-GC, Bruker; column 30 m, 0.25 mm, 0.25 µm HP-5-MS) with He (carrier gas) inlet pressure programmed for a constant flow of 0.6 mL/minute and mass spectrometric detector [SCION TQ, Bruker; 70 eV, mass to charge (m/z) ratio of 50–700]. The injector temperature was set at 230°C. The GC temperature program for the first method was as follows: injection at 70°C, oven 1 minute at 70°C, raised by 9°C/minute to 320°C, and held for 10 minutes at 320°C with a pressure pulse of 12 psi during 1 minute. The second method was carried out with the temperature program: injection at 60°C, oven 1 minute at 60°C, raised by 5°C/minute to 320°C, and held for 10 minutes at 320°C. The inlet pressure was programmed for a constant flow of 1 mL/minute with a pressure pulse of 30 psi for 1 minute. The injector and mass spectrometric detector sets were the same for both methods. For differential analysis, the raw data were pre-processed with xcmsonline website. The m/z fragments of interest were then tentatively identified on the basis of their mass spectra and their retention index. The

mass spectrum of compounds was compared with the spectrum of known compounds stored in the NIST and Wiley libraries. We consider that a molecule is present if it is detected at least three times in a replicate.

Statistical analyses

Statistical analysis of the metabolomics data set was performed in Metaboanalyst 5.0 using the area of the peaks as the unit of reference. To comply with the small number of samples, a Wilcoxon rank sum test was performed for comparison of the samples by pairs (e.g., early-log DBT versus early-log $MgSO_4$). A fold change threshold of 2 and −2 was used to determine the differential metabolites, with a *P*-value ≤ 0.05. Then the annotated metabolites were also analyzed using PCA test which was built considering the different metabolites as individuals and the growth phases as variables. The PCA results indicate that the two first axis represent 50% of the data set inertia (variability of the data cloud). Finally, the metabolites intensities were also graphically presented for each growth phase using boxplots drawn in the software R (4.0).

Oligotrophic growth of *R. qingshengii* IGTS8

To test whether *R. qingshengii* IGTS8 is capable of oligotrophic growth, we cultured it in CDM (100 mL in 250-mL baffled flasks) with 0.1 mM DBT as the main sulfur source without the addition of the carbon source glucose. To exclude ethanol (the DBT solvent) from the cultures, we adopted two different methods. In the first method, DBT was added to an empty sterile flask and ethanol was evaporated either at room temperature for 30 minutes or on a hot plate at 40°C for 15 minutes in a biological safety cabinet. When the DBT crystals appeared at the bottom of the flask and the liquid ethanol (100 µL) was not visible, we assumed that ethanol was completely evaporated. The culture medium which was prepared in another flask was then transferred to the flask containing DBT. In the second method, DBT (1.84 mg) was directly added to the culture medium as solid crystals (without ethanol). To check whether the oligotrophic growth is induced under biodesulfurization conditions, control cultures were run in parallel containing 0.1 mM $MgSO_4$ or DBT as the main sulfur source with and without ethanol addition. When ethanol was added (100 µL), it was evaporated as described above. Furthermore, another set of cultures was prepared in CDM lacking both the carbon and sulfur sources (neither glucose, ethanol, DBT nor $MgSO_4$ was added). Growth was followed by optical density measurements at 600 nm (OD_{600}) every 24 hours over an incubation period of 7 days. Biodesulfurization of DBT was tested in culture samples after 7 days of incubation using GC-MS as described (38). All cultures were prepared in biological triplicates, inoculated with single colonies from LB agar plates, and incubated for 7 days at 30°C in an orbital shaker. All experiments were repeated at least three times. In addition, oligotrophic growth of the strain IGTS8 was investigated on plates of CDM solidified with agar (16 g/L). Glucose and ethanol were excluded from all plates, which contained either DBT (added as solid crystals, 1.84 mg/100 mL medium) or $MgSO_4$ (0.1 mM) as the main sulfur source. Control plates were prepared without the addition of any carbon or sulfur sources. Furthermore, positive control plates contained glucose (10 mM), ethanol (0.1%), and 0.1 mM of either DBT or $MgSO_4$. All plates were prepared in duplicates, streaked with single colonies from LB agar plates, and incubated at 30°C for 7 days.

Growth of *R. qingshengii* IGTS8 on glycerol

To test the effect of the carbon source on the growth of *R. qingshengii* IGTS8 under biodesulfurization conditions, it was cultured in CDM (100 mL in 250-mL baffled flasks) containing 0.5 mM DBT and either glucose (20 mM) or glycerol (40 mM) as a carbon source. The concentration of glucose and glycerol was adjusted to have a final carbon concentration of 120 mM in both cultures. Ethanol (0.5%, vol/vol) was present in both cultures as the co-solvent of DBT. The glucose and glycerol cultures were inoculated from

the respective precultures to have a starting biomass load of 0.3 mg/L. All cultures were run in biological triplicates at 30°C in an orbital shaker (180 rpm). Growth was followed by OD_{600} every 24 hours.

Transmission electron microscopy

Cell pellets were harvested from 1 mL of the DBT and $MgSO_4$ cultures during the early-log, mid-log, and stationary phase. After washing with deionized water, cells were fixed overnight at 4°C with a solution containing glutaraldehyde (2.5%), and subsequently rinsed three times with phosphate buffer (0.1 M, pH 7.2). An additional fixation step was conducted with a solution containing osmium tetroxide (1%) for 1 hour at room temperature. Finally, increasing concentrations of water/ethanol solutions (35%, 50%, 70%, 85%, 95%, and 100%) were added to the cells to dehydrate them by washing the cells for 10 minutes two times. Each cell pellet was washed with 1 mL of propylene oxide (>99.5% vol/vol) for 5 minutes. Bacterial cells were then infiltrated at room temperature with a mixture of ethanol:epoxy resin which was prepared as described by the manufacturer's protocol. Thereafter, the bacterial cells were further infiltrated by epoxy resin:ethanol 1:3 for 1 hour, 1:1 for 2 hours, and 100% resin for 4 hours at room temperature. Resin polymerization occurred during further incubation at 70°C for 12 hours. The resulting resin blocks were ultrathin-sectioned and mounted onto copper slot grids. Thin sections were imaged using a ThermoFisher Talos L120C G2 TEM operating at 120 kV. All the reagents were purchased from Electron Microscopy Science.

Surface tension measurement

To check the IGTS8 cultures for biosurfactants production, the surface tension was measured in cell-free supernatants collected from the DBT and $MgSO_4$ cultures (two biological replicates) at time intervals at room temperature with a Kruss K100MK3 Tensiometer (Kruss, Germany) equipped with a platinum plate via the Wilhelmy plate method. The tensiometer was calibrated by adjusting the measurement so that the surface tension of water is 72 mN/m. The data were analyzed by one-way analysis of variance using Tukey's multiple comparisons test and applying a significance level of $P < 0.05$, using GraphPad Prism 6 (Trial Version).

RESULTS AND DISCUSSION

An overview of the proteomics and metabolomics data

Of the 6,734 proteins encoded by the *R. qingshengii* IGTS8 genome, we identified 2,896 proteins (43% of the total proteome) in our shotgun proteomics analyses of the DBT and $MgSO_4$ cultures. The relative abundance of many of these proteins varied significantly depending on the sulfur source and growth phase (Tables S1 and S2), and most of the differentially produced proteins (about 70%) were significantly more abundant in the DBT culture. Only 1,089 proteins could be grouped into functional categories using GO terms from the Gene Ontology database (Fig. 1; Fig. S2; Table S2). These proteins cover all major metabolic and physiological processes including the metabolism of carbohydrates, amino acids, lipids and fatty acids, nucleotides, vitamins and cofactors, protein synthesis, nucleic acids processing, stress response, energy metabolism, cell envelope biogenesis, and cell division. The majority of the categorized proteins (39%) were classified under the category "ATP-binding proteins," followed by the categories "protein metabolism" (19%) and "lipid metabolism" (11%). Members of the ATP-binding proteins category perform putative functions related to ATP binding/hydrolysis, for example, ABC-type transporters, kinases, helicases, carboxylases, recombinases, proteases, ligases, and chaperons. This protein category constituted the majority of the upregulated proteins in the DBT culture followed by protein metabolism, lipid metabolism, amino acid metabolism, and carbohydrate metabolism. In contrast, the majority of the downregulated proteins were involved in carbohydrate metabolism, followed by lipid metabolism, ATP binding, and protein metabolism. GO (biological process) enrichment analysis revealed temporal

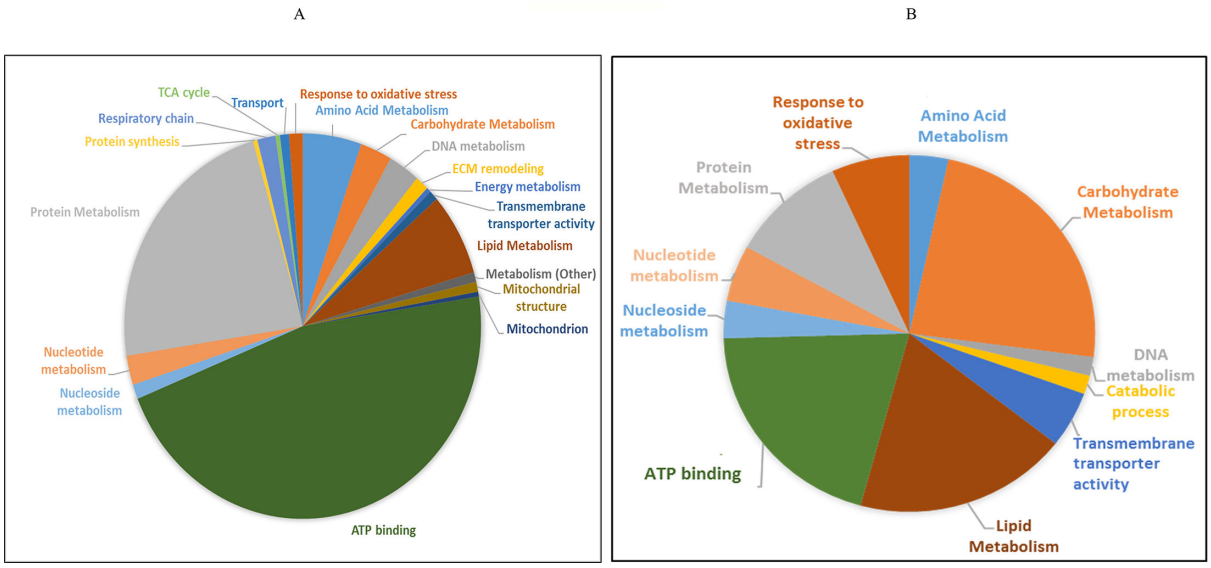

FIG 1 Functional classification of differentially produced proteins in *R. qingshengii* IGTS8 during the mid-log phase. (A) Proteins upregulated in the DBT culture. (B) Proteins downregulated in the DBT culture. The names of the protein functional categories are generic terms according to the Gene Ontology database. Therefore, the same functional category can be found in the upregulated and downregulated protein groups, which refer to different proteins belonging to the same category. ECM: extracellular matrix (molecular function of this category is metal ion binding).

variations in terms of the number and type of the enriched functional protein categories, the number of proteins in each enriched category, and the fold enrichment (Fig. S3). A total of 140 metabolites were detected in the metabolome (Fig. S4 and S5; Tables S3 through S5). The relative abundance of many metabolites varied significantly with the sulfur source and growth phase. The most significant differences were observed for metabolites of lipids, amino acids, as well as vitamins and cofactor metabolism.

PCA of the proteomics and the metabolomics data revealed distinct clusters for the DBT and $MgSO_4$ cultures (Fig. S6 and S7). These results demonstrate a global and versatile response of *R. qingshengii* IGTS8 under biodesulfurization conditions which, to our knowledge, has not been reported to this extent for a biodesulfurizing bacterium.

Reorganization of central metabolism: induction of the glyoxylate shunt

With only a few exceptions, the levels of central metabolism proteins were either significantly lower in the DBT culture throughout all growth phases or not significantly different between the two cultures, including enzymes of glycolysis (Embden-Meyerhof-Parnas and pentose phosphate pathways) and the tricarboxylic acid cycle (TCA) cycle (Fig. 2; Tables S1 and S2). The lower abundance of glycolytic and TCA cycle enzymes explains the lower specific growth rate of *R. qingshengii* on DBT (19). On the contrary, isocitrate lyase, a key enzyme of the glyoxylate shunt, was up to 26-fold more abundant in the biodesulfurizing culture and maintained its increased abundance throughout all growth phases (Fig. 2). However, the other key enzyme of the glyoxylate shunt, malate synthase, was significantly less abundant in the biodesulfurizing culture during the late-log and stationary phases (Tables S1 and S2). The glyoxylate shunt is usually activated under carbon starvation and when the TCA cycle is arrested due to nutrients and oxygen limitations (39). Induction under sulfate starvation or biodesulfurization conditions has not been reported to our knowledge.

The abundance of isocitrate lyase increased in *Rhodococcus jostii* RHA1 during carbon starvation in the stationary phase (25). Isocitrate lyase and malate synthase were more abundant in propane-grown cultures of *Mycobacterium* sp. strain ENV421 and *Rhodococcus* sp. strain ENV425 compared to succinate-grown cultures. Upregulation of the glyoxylate shunt enzymes was correlated with the net production of acetyl-CoA from

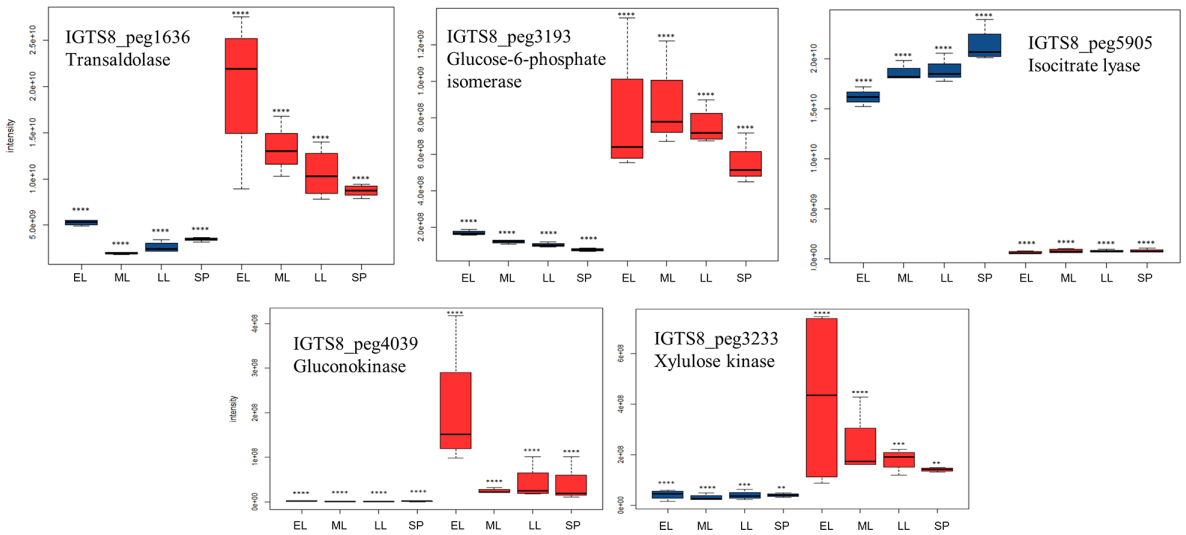

FIG 2 Boxplots of the label-free quantification (LFQ) values showing the abundance profile of some central metabolism proteins in the dibenzothiophene (DBT, in blue) and inorganic sulfate ($MgSO_4$, IS, in red) cultures. To show the distribution of the samples, all of them were considered (this applies to all subsequent figures). The growth phases are abbreviated as EL (early-log), ML (mid-log), LL (late-log), and SP (stationary phase). Significance is attested by a Limma moderated *t*-test as follows: no * $P > 0.05$, *$P \leq 0.05$, **$P \leq 0.01$, ***$P \leq 0.001$, ****$P \leq 0.0001$.

propane (40). In addition, changes in the metabolic flux through the central metabolism pathways occurred and isocitrate lyase was much more abundant when *Rhodococcus opacus* PD630 was grown on phenol instead of glucose (41). In *Mycobacterium tuberculosis*, the glyoxylate shunt was shown to be essential for fatty acid catabolism, virulence, and survival (42). Moreover, isocitrate lyase is essential for growth under glycerol-limited conditions and was proposed to be a key enzyme in a novel carbohydrate metabolic route (43). Various physiological functions of the glyoxylate shunt have been reported including detoxification of glyoxylate, utilization of triacylglycerols, and replenishment of oxaloacetate during growth on acetate or fatty acids (39). It also avoids the loss of CO_2 in the oxidative arm of the TCA cycle, preserves CoA units during oligotrophic growth, and links gluconeogenesis to the oxidation of acetyl residues resulting from fatty acid degradation (39).

Although we have no direct clues as to why the abundance of isocitrate lyase increased in the DBT culture, we can hypothesize some scenarios based on our omics data and the literature. The first scenario is related to a higher oxygen demand in the biodesulfurizing culture which is needed to retrieve sulfur from DBT via the 4S pathway. Hence, the biodesulfurizing culture might experience hypoxia, which is known to induce the glyoxylate shunt (39). The other scenario deals with the presence of glucose as a carbon source in the biodesulfurizing culture. In general, higher energy demand in bacteria stressed with aromatic substrates (like DBT) was reported (41). Moreover, it is known that there is a higher energy demand during desulfurization via the 4S pathway where each mole of DBT requires 4 moles of NADH (44, 45). This extra NADH can be more readily supplied from ethanol via alcohol dehydrogenase, which makes ethanol superior to glucose as a carbon source in terms of a higher growth yield and specific desulfurization activity (44–46). Accordingly, the specific combination of glucose and DBT in the biodesulfurizing culture may induce a type of carbon nutritional stress that leads to increased synthesis of the glyoxylate shunt enzymes.

To determine whether glucose was causing any growth defects in the DBT culture, we grew strain IGTS8 on glycerol as an alternative carbon source in the presence of the same DBT concentration added in the glucose culture. We noticed a slightly higher OD_{600} and growth rate for the glycerol culture (Fig. S8). However, both the OD_{600} and specific growth rate of the glycerol culture (0.072/hour) were not significantly different from that of the glucose culture (0.066/hour). Although these results rule out growth disadvantage

in the glucose culture, a potential nutritional stress cannot be completely excluded. Therefore, we postulate that the biodesulfurizing culture could benefit from the available ethanol (DBT solvent, 0.5%) as a source of the required reducing equivalents (NADH). This reasoning is backed by the higher abundance of several alcohol dehydrogenases in the DBT culture such as IGTS8_peg1280 and IGTS8_peg6110 (Tables S1 and S3). If ethanol were further oxidized to acetate, the glyoxylate shunt would be required for further metabolism.

In addition to the enzymes that operate the oxidative TCA cycle, a putative citrate lyase, a key enzyme of the reductive TCA cycle, was significantly more abundant (up to 17-fold) in the biodesulfurizing culture, and its level increased toward the stationary phase. In general, the level of most carbohydrate metabolism enzymes was significantly lower in the DBT culture, consistent with the metabolome profile (Fig. 2; Tables S3 through S5).

An NADP-dependent malic enzyme appears to be a key metabolic link between glycolysis, gluconeogenesis, and the TCA cycle, which is controlled by the metabolic switch or anaplerotic node (phosphoenolpyruvate-pyruvate-oxaloacetate node) (47). This is inferred from the observation that malic enzyme was significantly more abundant in the DBT culture, whereas the relative abundance of both phosphoenolpyruvate carboxykinase and pyruvate carboxylase was not significantly different between the DBT and $MgSO_4$ cultures (Tables S1 and S2). The malic enzyme catalyzes the oxidative decarboxylation of malate to produce pyruvate and NADPH, which is crucial for anabolic processes (39). Further discussion on central metabolism is included in the Supplementary Material.

Oligotrophy in the biodesulfurizing culture of *R. qingshengii* IGTS8

Oligotrophy is a common phenotype among some representatives of the genera *Rhodococcus* and *Streptomyces*. It is usually induced, and allows the utilization of atmospheric CO_2 and CO, under carbon starvation (48). The biodesulfurizing culture of *R. qingshengii* IGTS8 was highly enriched (up to 170-fold) during all growth phases in two polypeptides annotated as carbon monoxide dehydrogenase D (IGTS8_peg6111) and E (IGTS8_peg6112) proteins (Fig. S9; Tables S1 and S2). The former is identical to an ATPase of the MoxR family from several *Rhodococcus* spp., which is known as a modulator of stress response pathways and may have a chaperone-like role in the maturation of proteins and insertion of cofactors (49, 50). MoxR homologs are important for the formation of active methanol dehydrogenase in *Paracoccus denitrificans* (51) and maturation of CO dehydrogenase in *Oligotropha carboxidovorans* (52). IGTS8_peg6112 is identical to uncharacterized proteins from *Rhodococcus* spp. that belong to the conserved von Willebrand factor type A domain protein family (Pfam 05762, VWA_CoxE). CoxE-like proteins are found in several bacteria as a part of their CO-oxidizing systems (53) where they may be involved in post-translational assembly of the CO dehydrogenase bimetallic cluster (54) or in protein-protein interactions (55). The arrangement of the genes encoding the MoxR and CoxE homologs is consistent with the observation that ATPases of the MoxR family are commonly encoded upstream of a gene encoding a von Willebrand factor type A domain-containing protein (49, 50).

R. qingshengii IGTS8 *moxR* and *coxE* reside in an operon downstream of the gene for methanol:*N*, *N*´-dimethyl-4-nitrosoaniline oxidoreductase (ThcE, IGTS8_peg6110, UniProtKB-Q53062) which catalyzes the oxidation of methanol to formaldehyde (56) and was significantly more abundant in the DBT culture (up to 46-fold) at all growth phases. In *R. erythropolis* N9T-4, ThcE was induced during growth in aminutesimal medium without a carbon source (oligotrophic growth) and was proposed to be a part of a CO_2 fixation pathway involving methanol/formaldehyde (57). Notably, under the same conditions, an aldehyde dehydrogenase was highly abundant (57, 58), an ortholog of which is encoded downstream of the genes of the mycofactocin system of *R. qingshengii* IGTS8 (discussed below).

We postulate that MoxR/CoxE/ThcE orthologs are involved in C1 metabolism in *R. qingshengii* IGTS8, where ThcE may be an alcohol dehydrogenase and MoxR/CoxE may contribute to its maturation. The possibility that these proteins constitute a CO dehydrogenase can be excluded because none of them shows homology to the major structural subunits (CoxL, CoxM, and CoxS) of known CO dehydrogenases (53). In the meantime, we do not exclude the ability of *R. qingshengii* IGTS8 to utilize CO/CO_2 as a carbon and energy source. Patrauchan et al. (25) reported higher activity and abundance of CO dehydrogenase in carbon-starved stationary phase cells of *R. jostii* RHA1. The proteins IGTS8_peg4820-IGTS8_peg4823 probably constitute the three structural subunits of a putative CO dehydrogenase as well as a related protein annotated as carbon monoxide dehydrogenase G protein (53). However, only the latter protein was detected in the proteome and there was no significant difference in its abundance. Assuming that *R. qingshengii* IGTS8 indeed possesses a CO dehydrogenase, then MoxR/CoxE may constitute its post-translational maturation chaperone (52, 54).

C1 metabolism in the biodesulfurizing *R. qingshengii* IGTS8 can furthermore be inferred from our previous finding that a NAD/mycothiol-dependent formaldehyde dehydrogenase had a slightly higher level in the presence of DBT (19, 59), suggesting a role in formaldehyde dissimilation. In *R. erythropolis* N9T-4, the gene encoding an ortholog of the NAD/mycothiol-dependent formaldehyde dehydrogenase is remarkably expressed in the presence of formaldehyde (60). Furthermore, the glyoxylate shunt enzymes were reported to play a role in oligotrophic growth in *R. erythropolis* N9T-4 (61), consistent with the higher abundance of isocitrate lyase in the DBT culture of *R. qingshengii* IGTS8.

The higher abundance of putative C1 metabolism and oligotrophy-related enzymes in the DBT culture raises the questions: can *R. qingshengii* IGTS8 grow oligotrophically? and does this metabolic trait play any role under biodesulfurization conditions? To find out whether *R. qingshengii* IGTS8 is capable of oligotrophic growth, we cultured it in CDM lacking carbon and energy sources (glucose) in the presence of DBT as the main sulfur source after evaporating the co-solvent of DBT (ethanol). Interestingly, IGTS8 grew under these conditions, reaching an average OD_{600} of 0.36 after 3 days (Fig. S10), unlike other reported oligotrophs that can grow only on solid media (48). The average OD_{600} increased to 0.46 within 7 days and reached 0.6 in one biological replicate. We observed considerable variations in the OD_{600} between the biological replicates and among the repeated cultures. GC-MS analysis after 7 days confirmed the utilization of DBT and production of 2-hydroxybiphenyl, the typical product of the 4S biodesulfurization pathway (1–3) (Fig. S11), indicating the functionality of the 4S pathway under oligotrophic conditions. *R. qingshengii* IGTS8 did not grow when DBT was replaced by $MgSO_4$ (even after 1 month of incubation) or in a medium lacking both carbon and sulfur sources (Fig. S10).

These findings demonstrate the ability of *R. qingshengii* IGTS8 to grow oligotrophically and suggest that this phenotype might be induced under biodesulfurization conditions, consistent with the upshift of putative C1 metabolism enzymes in the DBT culture such as a putative carbonic anhydrase, 5-formyltetrahydrofolate cyclo-ligase, methylenetetrahydrofolate dehydrogenase, and 5,10-methylenetetrahydrofolate reductase, in addition to several aldehyde dehydrogenases (Tables S1 and S2) (48). These results, however, raise the question: what was the carbon and energy source that allowed the DBT culture to grow? Although ethanol in the DBT culture was evaporated before inoculation, it was crucial to determine if it has an effect on oligotrophy as it was recently reported to induce oligotrophy-related enzymes in *R. erythropolis* N9T-4 (62), knowing that the IGTS8 strain can grow on ethanol as a sole carbon and energy source. Therefore, we cultured the IGTS8 strain in CDM lacking glucose with $MgSO_4$ as the main sulfur source and ethanol was added and then evaporated before inoculation as we did with the DBT culture. The growth profile of this culture was similar to that of the corresponding DBT culture (Fig. S10), indicating that the observed growth in the glucose-free DBT or $MgSO_4$ cultures is correlated with the addition of ethanol. But how ethanol could play

a role although it was evaporated from the cultures before inoculation? It appears that some ethanol molecules were trapped in the headspace of the cultures and these could support the observed growth.

Since we have no control over the amount of ethanol molecules trapped in the headspace, this amount could be variable which explains the large differences in the OD_{600} between the biological replicates. Accordingly, we postulate that *R. qingshengii* IGTS8 can utilize ethanol from the gas phase of the cultures, and in that case, ethanol may serve both as a carbon/energy source and/or an inducer of oligotrophy enzymes. To confirm our hypothesis, we cultured the IGTS8 strain in CDM with either $MgSO_4$ or DBT without glucose, and ethanol was fully excluded from the culture medium by adding DBT in the form of solid crystals. These cultures failed to grow within 7 days of incubation, further confirming the importance of ethanol.

Assuming that ethanol remaining in the headspace of the liquid cultures was utilized as a carbon and energy source, we can still propose oligotrophy in *R. qingshengii* IGTS8 because prior evaporation of ethanol excludes the presence of a high ethanol concentration in the cultures, thus creating the main trigger of oligotrophy, namely carbon starvation (4). However, results from the liquid cultures provide no clues as to the activation or induction of oligotrophy under biodesulfurization conditions (in the DBT culture). To get deeper insights into this aspect, we cultured the strain IGTS8 on plates of CDM solidified with agar, which supports better growth of oligotrophs than in the liquid medium (48). Interestingly, the strain IGTS8 grew on plates without glucose and ethanol where DBT was added as solid crystals (Fig. S12 through S16). On these plates, single colonies started to appear after 3 days of incubation and continued to increase in size up to day 7. The colony size was smaller, and the growth was slower, compared to cultures grown on plates containing glucose, ethanol, and DBT, which can be reconciled. These findings provide several clues. First, the strain IGTS8 is capable of oligotrophic growth, confirming the outcome of the liquid cultures. Second, ethanol is not required for oligotrophy on a solid medium, on contrary to liquid cultures. To answer the question of whether oligotrophy is induced under biodesulfurization conditions, we cultured the strain IGTS8 on CDM agar plates lacking glucose and ethanol in the presence of $MgSO_4$ as the main sulfur source. This culture gave scarce growth which was weaker and slower compared to growth on the DBT crystal plates. Single colonies could be clearly recognized only after 6 days of incubation, suggesting better oligotrophic growth under biodesulfurization conditions. Oligotrophic growth on plates lacking glucose and ethanol raised a question about the carbon and energy sources that the strain IGTS8 utilized. *R. qingshengii* IGTS8 did not show prominent growth on CDM agar plates lacking carbon (glucose and ethanol) and sulfur (DBT, $MgSO_4$) sources within 7 days of incubation, showing that it cannot utilize agar as a source of the lacking nutrients. This finding renders the utilization of atmospheric CO/CO_2 as the most plausible explanation of the observed oligotrophic growth on the CDM agar plates. However, these postulations await further studies to be validated.

Although we showed that *R. qingshengii* IGTS8 is capable of oligotrophic growth under carbon starvation in the presence of DBT, it is uncertain whether oligotrophy or heterotrophic CO/CO_2 assimilation occurred in the biodesulfurizing cultures which had plenty of carbon (glucose and ethanol), thus excluding the main trigger of oligotrophy, namely carbon starvation. Increase in the abundance of putative C1 and oligotrophy-related enzymes could be a nonspecific stress response to sulfate limitation stress in the DBT culture or to the presence of ethanol, which was reported to induce oligotrophic enzymes (62). Alternatively, as we reasoned above for the glyoxylate shunt, a potential glucose-induced nutritional stress that occurs only in the DBT culture could urge the biodesulfurizing cells to use additional resources to meet their demand for energy and reduce equivalents. The glyoxylate shunt could be important under these conditions to avoid the loss of CO_2 in the oxidative arm of the TCA cycle and to preserve CoA units (39, 48, 61).

A higher abundance of C1 metabolism and oligotrophy-related enzymes under biodesulfurization conditions could support energy scavenging for survival or persistence (63). In oleaginous bacteria (including *Rhodococcus* spp.), CO_2 assimilation via anaplerotic reactions under heterotrophic conditions could be crucial for the biosynthesis of triacylglycerols and odd-numbered fatty acids which are enriched in triacylglycerols (64). While oligotrophy in the DBT culture appears consistent with the higher production of the glyoxylate shunt key enzyme isocitrate lyase (61), it remains to be determined whether CO or CO_2 uptake and metabolism actually occurred and what the implications of this "mixotrophic" phenotype (63) might be during biodesulfurization. It is worth noting that the molecular mechanisms regulating oligotrophy and the underlying CO_2 fixation pathways and carbon metabolism have not been elucidated (48).

The mycofactocin system is highly induced in the biodesulfurizing culture

One of the most interesting and genuine findings of our study is the strong upshift of the mycofactocin biosynthesis and associated proteins in the DBT culture, a response that has not been reported in biodesulfurizing or sulfate-deprived bacteria (Fig. 3; Tables S1 and S2). Mycofactocin is a glycosylated redox cofactor that is ribosomally synthesized and post-translationally modified. It is commonly found in *Mycobacterium* spp. and other *Actinomycetota* including rhodococci (65). Among the mycofactocin biosynthesis proteins, MftB (IGTS8_peg6132), MftC (IGTS8_peg6133), and MftD (IGTS8_peg6134) were much more abundant in the DBT culture during all growth phases with a fold change ranging from 9.9- to 4,096-fold. These levels did not vary remarkably with the growth phase. In fact, the radical *S*-adenosylmethionine enzyme MftC, which catalyzes the first step of mycofactocin biosynthesis (modification of the precursor peptide MftA) (Fig. S17) exhibited the highest fold change among all identified proteins (fold change = 1,520 to 4,337). In addition to the mycofactocin biosynthesis proteins, the *R. qingshengii* IGTS8 mycofactocin gene cluster encodes several putative mycofactocin-associated oxidoreductases (65, 66), two of which (IGTS8_peg6137 and IGTS8_peg6144) were also significantly more abundant under biodesulfurization conditions (up to 55.7-fold and 20-fold, respectively). IGTS8_peg6144 is located downstream of the mycofactocin gene cluster and is probably encoded in a separate operon because it is preceded by a gene encoding a putative transcriptional regulator. The IGTS8_peg6144 is identical to *S*-ethyldipropylcarbamothioate-inducible aldehyde dehydrogenase (ThcA) from *R. erythropolis* (UniProtKB-P46369), which degrades aldehydes produced by *N*-dealkylation of thiocarbamates (67). Notably, IGTS8_peg6144 is an ortholog of the aldehyde dehydrogenase that is highly induced during oligotrophic growth of *R. erythropolis* N9T-4 (58).

The physiological functions of mycofactocin are being explored, and roles in survival under hypoxia, redox homeostasis, as well as glucose and alcohol metabolism have been reported (65, 66, 68). Recently, the role of mycofactocin in glucose metabolism in *M. tuberculosis* was inferred from the reduced activity of $NADP^+$-glucose-6-phosphate dehydrogenase in a Δ*mftD* mutant (68). The authors suggested that mycofactocin may serve as an external redox exchange system for $NADP^+$-glucose-6- phosphate dehydrogenase under oxygen limitation. A similar role in glucose metabolism could be proposed for the strain IGTS8.

Consistent with the higher abundance of putative C1 metabolism enzymes and proposed oligotrophy in the DBT culture, a mycofactocin system-associated transcriptional regulator was shown to regulate the expression of genes encoding the NAD-dependent aliphatic aldehyde dehydrogenase (ThcA) and *N*, *N*′-dimethyl-4-nitrosoaniline-dependent methanol dehydrogenase (ThcE) (58), which are highly expressed *in Rhodococcus erythropolis* N9T-4 under oligotrophic conditions, as their orthologs identified here. Furthermore, mycofactocin serves as an electron acceptor of methanol dehydrogenase in the methylotroph *Mycobacterium smegmatis* (69). Therefore, we propose a role for the mycofactocin system in oligotrophy or C1 metabolism in *R. qingshengii* IGTS8. It is also possible that the upshift in mycofactocin production in the

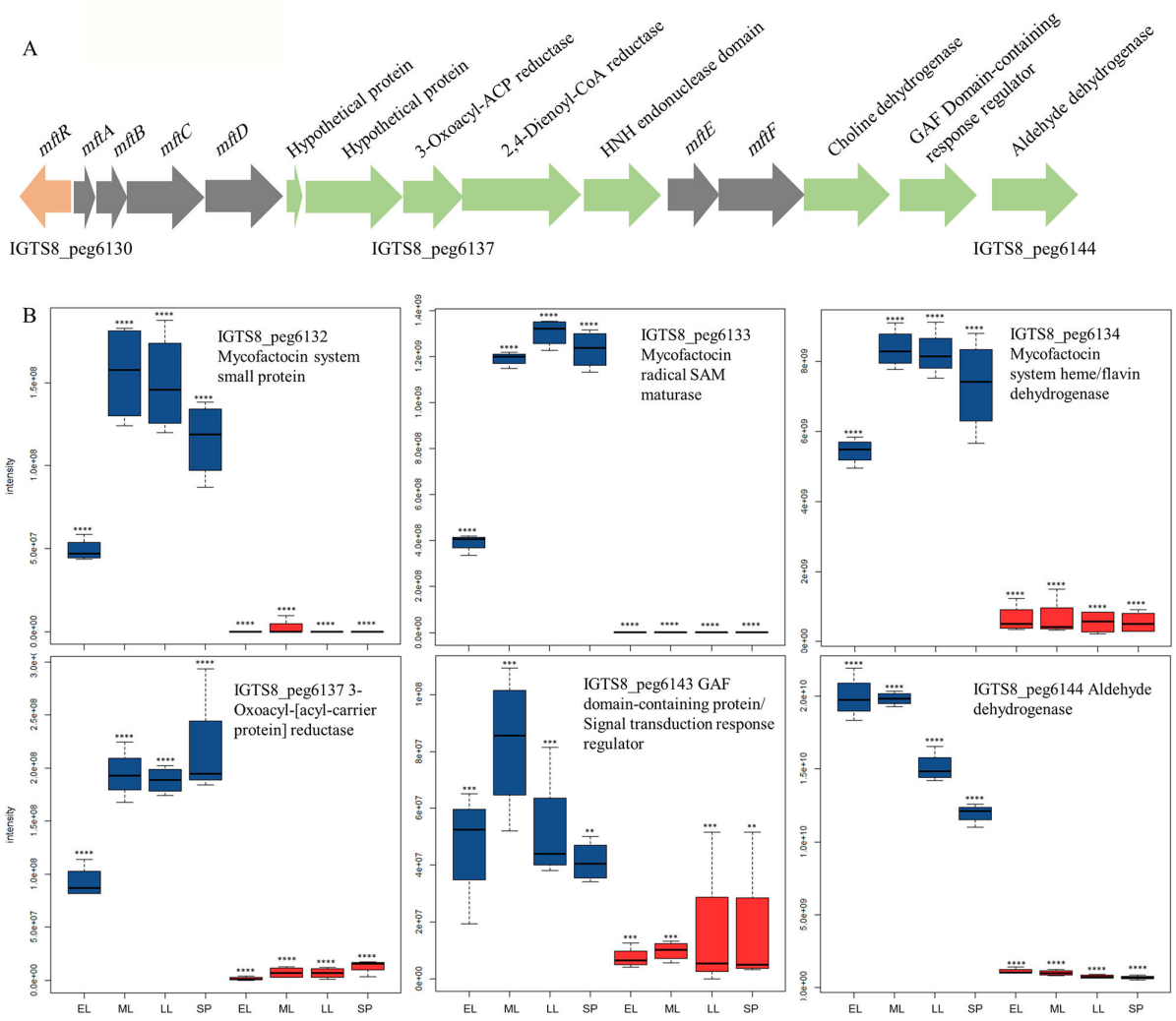

FIG 3 (A) A gene cluster encoding the mycofactocin system (gray arrows) and associated proteins (green arrows) in *R. qingshengii* IGTS8. (B) Boxplots of the label-free quantification (LFQ) values showing the abundance profile of the mycofactocin system and associated proteins in the dibenzothiophene (DBT, in blue) and inorganic sulfate ($MgSO_4$, IS, in red) cultures. The growth phases are abbreviated as EL (early-log), ML (mid-log), LL (late-log), and SP (stationary phase). Significance is attested by a Limma moderated *t*-test as follows: no * $P > 0.05$, *$P \leq 0.05$, **$P \leq 0.01$, ***$P \leq 0.001$, ****$P \leq 0.0001$.

biodesulfurizing culture could be a response to the presence of ethanol, in line with its role in alcohol metabolism (69, 70). Based on the observed oxidative stress response in the DBT culture of *R. qingshengii* IGTS8 (19), a role for mycofactocin in redox balance could be envisaged. In accordance with its role as a redox cofactor, several mycofactocin-associated oxidoreductases were also more abundant in the DBT-grown cells of *R. qingshengii* IGTS8.

Cell envelope biogenesis and degradation

In view of the hydrophobicity (low bioavailability, aqueous solubility = 1.47 mg/L) (71) and potential toxicity of DBT (72), cell surface modifications could be expected as a stress response (73). Indeed, more than 40 differentially produced proteins related to cell envelope biogenesis and degradation were identified, thus constituting the largest functional category of proteins detected. These included many transglycosylases, transpeptidases, endopeptidases, murein hydrolases, and peptidoglycan biosynthesis and recycling enzymes, in addition to cell surface-associated proteins. More than 50% of those proteins, especially peptidoglycan biosynthesis and recycling proteins, were significantly less abundant under biodesulfurization conditions

(Tables S1 and S2), coinciding with the differential levels of cell wall/cell surface biosynthesis metabolites such as diaminopimelic acid, dTDP-D-fucosamine, trehalose, guanosine diphosphate mannose, and UDP-*N*-acetylmuramoyl-L-alanyl-D-glutamyl-6-carboxy-L-lysyl-D-alanyl-D-alanine (Tables S3 through S5).

Trehalose, which was less abundant in the DBT culture, is not only a key component of the cell envelope in rhodococci (trehalose mycolate) but also acts as a compatible solute, a stress protector, and a cell membrane stabilizer (73, 74). It is also a component of glycolipid biosurfactants produced by several *Rhodococcus* spp. (75), agreeing with the observed decrease in surface tension in both the DBT and inorganic sulfate cultures (Fig. S18). However, there was no statistically significant difference between the surface tension values of both cultures.

We detected several MCE (Mammalian Cell Entry) family proteins, mostly encoded in one operon, that were consistently depleted in the biodesulfurizing culture during all growth phases (Fig. 4A). Analysis of *R. qingshengii* IGTS8 genome revealed 26 MCE family members encoded mostly from gene clusters. These proteins are ubiquitous in *Proteobacteria* and *Actinobacteria* and constitute putative ABC-type transporters involved in lipid asymmetry in the cell membrane through the trafficking of phospholipids (76, 77). In *Actinomycetota*, a MCE4 protein is involved in cholesterol uptake (76, 77). However, it is hard to reconcile that MCE proteins could play a role in the uptake of DBT because they were strongly downregulated in the DBT culture.

Cell surface modifications are also evident by the higher abundance in the DBT culture of three enzymes (IGTS8_peg5608-IGTS8_peg5610) involved in fucose (O-antigen nucleotide sugar) biosynthesis. GDP-L-fucose is a component of the cell envelope lipopolysaccharides in rhodococci (78) (Fig. 4B). In *R. qingshengii* IGTS8, GDP-L-fucose can be produced from GDP-mannose which was relatively more abundant in the DBT culture starting from the mid-log phase. Another operon (IGTS8_peg1492-IGTS8_peg1494) encodes enzymes of lipoarabinomannan biosynthesis which were 3.5- to 6-fold more abundant in the DBT culture (Fig. 4B; Tables S1 and S2).

Biodesulfurization is associated with remodeling of the cell membrane composition

The type of sulfur source had a profound effect on lipid and fatty acid metabolism in *R. qingshengii* IGTS8 (Tables S1 and S2), with most of the enzymes involved being more abundant under biodesulfurizaiton conditions. Ethanolamine ammonia lyase was highly enriched (up to 904-fold) (Fig. 5A). Diacylglycerol and triacylglycerol/wax ester biosynthetic enzymes were generally more abundant, whereas the abundance of different types of lipases decreased in the presence of DBT (Tables S1 and S2). In line with the proteomics data, many metabolites of glycerophospholipid and fatty acid metabolism were differentially abundant (Tables S3 through S5). Ethanolamine and the monoacylglycerols 1-octadecanoyl-rac-glycerol (membrane stabilizer) and 1-hexadec-9-enoyl-sn-glycerol 3-phosphate were uniquely detected in the DBT culture (Fig. 5), whereas the levels of phosphatidylethanolamines (PEs) and all detected diacylgycerols were higher during growth on sulfate (Tables S3 through S5).

Remodeling of the cell membrane lipid composition is a common stress response in bacteria exposed to hydrophobic xenobiotics (like DBT, alkanes, aromatic compounds) and extremes of temperature, salinity, pH, and so on (73, 79), which is manifested in a process known as homeoviscous adaptation (80). Reducing the content of unsaturated fatty acids, particularly C16:1 and C18:1, as found in the DBT culture minimizes cell membrane fluidity and permeability, reminiscent of responses to high temperature (73, 79). *R. erythropolis* DCL14 responded to shifts in pH (from 7 to 3 and 11) and temperature (from 28°C to 4°C and 37°C) by increasing the degree of membrane fatty acid saturation (81). In addition, a relatively higher content of long-chain fatty acids (C16–C19) and a downshift of shorter fatty acids (C12–C14) in the DBT culture leads to increased hydrophobicity of the cell surface and also reduces the cell membrane fluidity (79). Chen et al. (82) reported increased cell surface hydrophobicity in *Gordonia* sp. SC-10 during

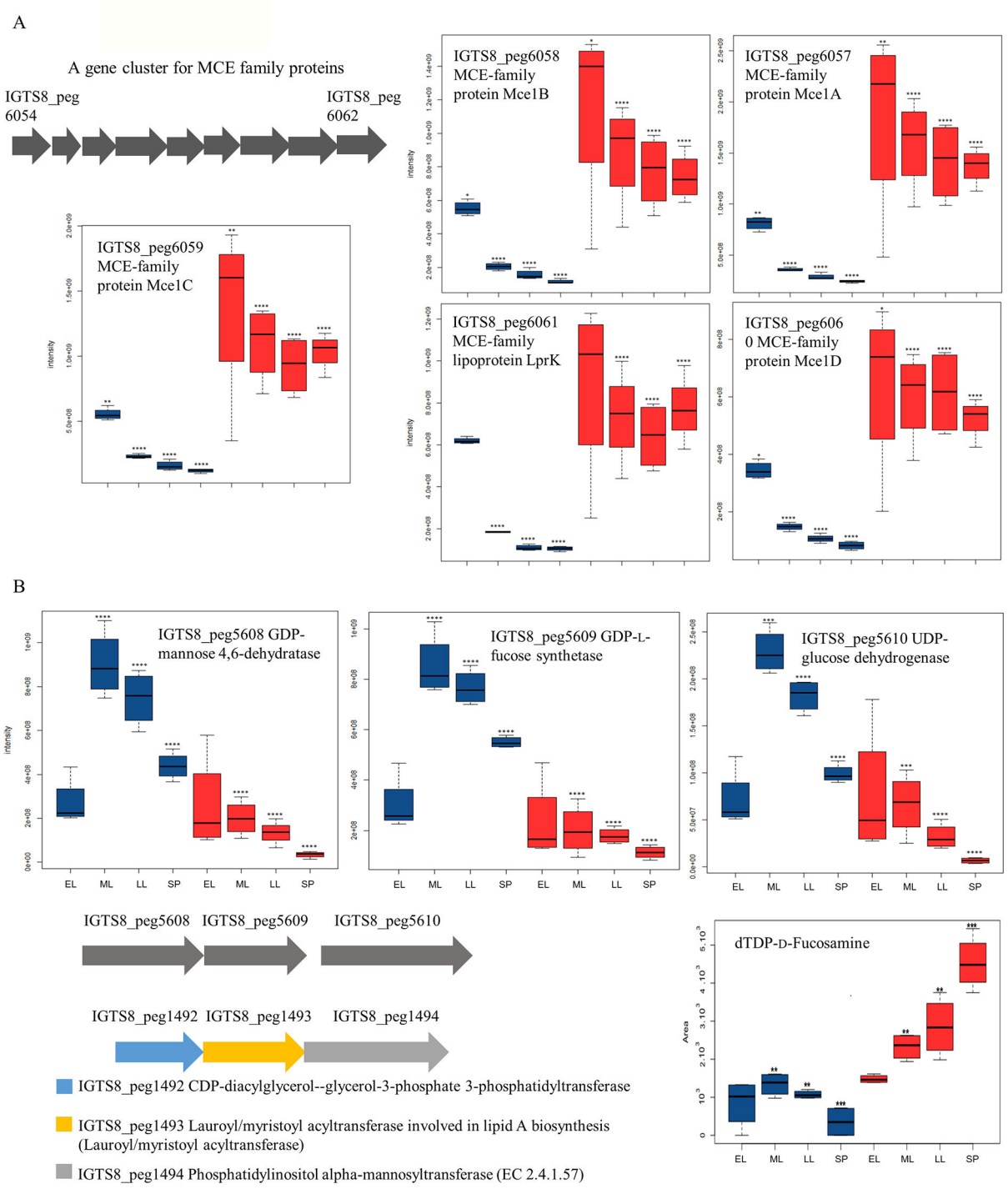

FIG 4 Boxplots of the label-free quantification (LFQ) values showing the abundance profile of cell surface (MCE family) (A) and cell envelope biogenesis proteins (B), as well as related metabolites and gene clusters, in the dibenzothiophene (DBT, in blue) and inorganic sulfate ($MgSO_4$, IS, in red) cultures. The growth phases are abbreviated as EL (early-log), ML (mid-log), LL (late-log), and SP (stationary phase). Significance is attested by a Limma moderated *t*-test as follows: no * $P >$ 0.05, *$P \leq 0.05$, **$P \leq 0.01$, ***$P \leq 0.001$, ****$P \leq 0.0001$.

biodesulfurization of diesel (in a biphasic system) compared to cells grown in aqueous cultures with sodium sulfate as the sole sulfur source, which was attributed to higher production of mycolic acids. Both responses are consistent with the hydrophobic nature of DBT and could simultaneously enable better substrate access and protection from hydrocarbon-associated toxicity (83).

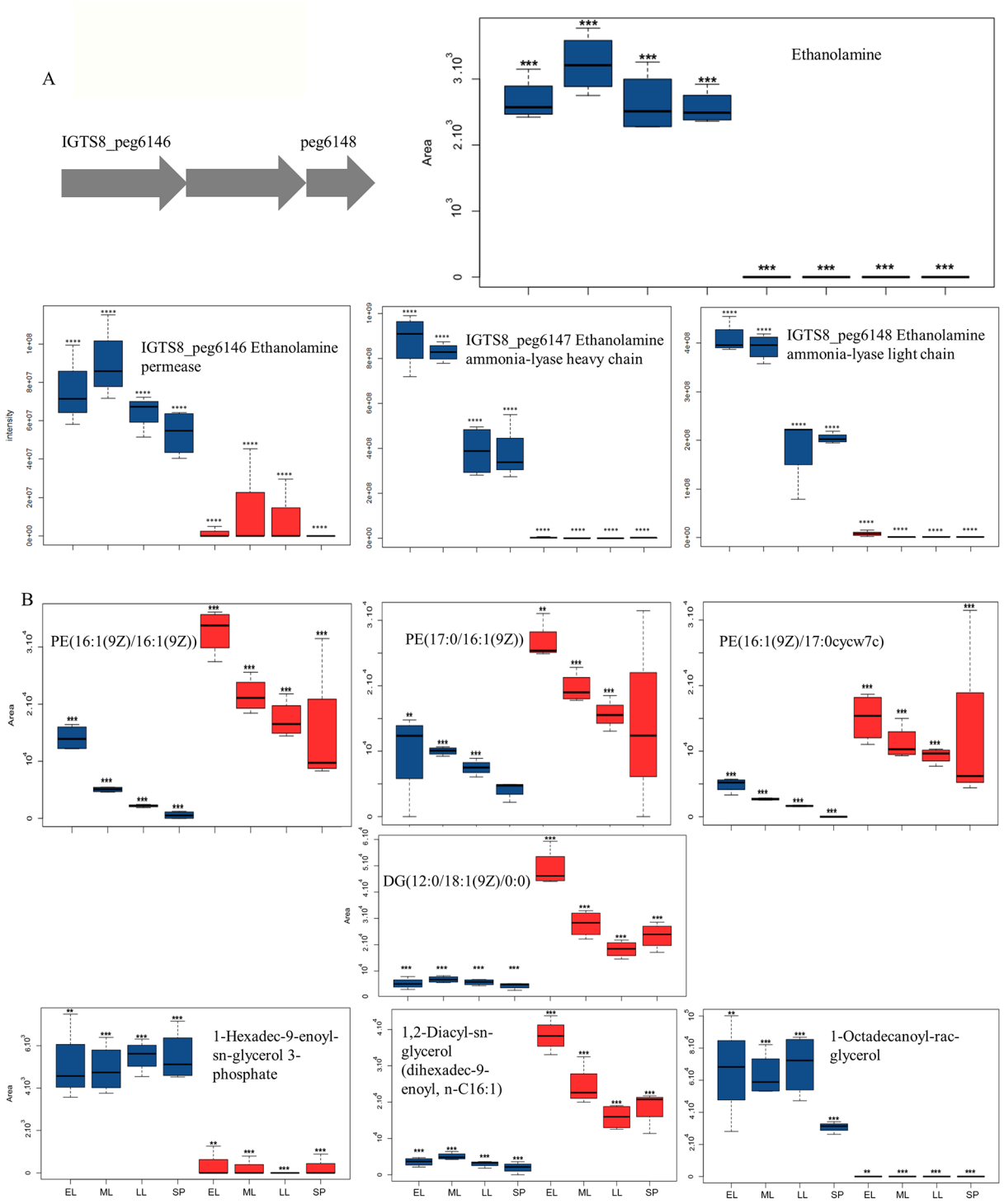

FIG 5 (A) A gene cluster encoding proteins of ethanolamine utilization and boxplots of the label-free quantification (LFQ) values showing the abundance profile of ethanolamine and ethanolamine ammonia lyase and (B) metabolites of lipid metabolism (PEs and acylglycerols) in the dibenzothiophene (DBT, in blue) and inorganic sulfate ($MgSO_4$, IS, in red) cultures. The growth phases are abbreviated as EL (early-log), ML (mid-log), LL (late-log), and SP (stationary phase). Significance is attested by a Limma moderated *t*-test as follows: no * $P > 0.05$, *$P \leq 0.05$, **$P \leq 0.01$, ***$P \leq 0.001$, ****$P \leq 0.0001$.

A decrease in cell membrane fluidity by increasing the content of saturated and long-chain fatty acids was also reported in the presence of high NaCl concentrations to prevent the leakage of solutes in halotolerant bacteria (81, 84). This trend of fatty acid changes is contrary to that observed in *Rhodococcus aetherivorans* BCP1 grown on

naphthenic acids where saturated fatty acids (C16:0 and C18:0) were of lower abundance compared to a glucose culture (85). Our observations do not fully agree with those of Watanabe et al. (86) who correlated an increase of the biodesulfurization activity with a higher fluidity of the cell membrane due to a reduced (28%–41%) level of 10-methyl fatty acids.

The downshift of PE content in the DBT culture (Fig. 5) suggested alterations in the head groups of phospholipids (79), consistent with the upregulation of enzymes involved in phosphatidylinositol metabolism and downregulation of enzymes catalyzing inositol degradation. The lower abundance of *myo*-inositol-2-phosphate in the DBT culture could be due to higher consumption in phospholipid biosynthesis. CDP-diacylglycerol-glycerol-3-phosphate 3-phosphatidyltransferase, involved in phosphatidylglycerol biosynthesis, was significantly more abundant in the DBT culture (87), indicating remodeling of the glycerophospholipids and modulation of cell surface charge as a stress response (81, 83). The cell membrane charge is a function of the relative proportions of zwitterionic glycerophospholipids like PE and the acidic phosphatidylglycerol (87).

The lower abundance of PEs in the DBT culture appears to contradict the significant upregulation of CDP-diacylglycerol-serine *O*-phosphatidyltransferase and phosphatidylserine decarboxylase, involved in PE biosynthesis, which could refer to regulation at the enzymatic activity level. Alternatively, consumption of PEs could be higher in the DBT culture as precursors for diacylglycerol, fatty acids, phosphatidic acid, and lipopolysaccharides (87). While the higher turnover rate of PEs could explain their lower abundance and exclusive detection of ethanolamine in the DBT culture, it is not clear why ethanolamine was still detectable in the DBT culture despite the presence of a much higher level of enzymes involved in its consumption (ethanolamine ammonia lyase). Notwithstanding this apparent discrepancy, the presence of ethanolamine and the upregulation of cobalamin biosynthesis enzymes further justify the higher abundance of ethanolamine ammonia lyase and aldehyde dehydrogenase catalyzing ethanolamine utilization (88). In the strain IGTS8, genes encoding ethanolamine utilization enzymes are located immediately downstream of the mycofactocin gene cluster, indicating a potential functional relationship.

Amino acid metabolism

Many enzymes of amino acid transport and metabolism were enriched in the DBT culture (Fig. 6; Tables S1 through S5). Glutamate and glutamate synthase were more abundant, which may be due to their key role in the biosynthesis of other amino acids, various cofactors, and secondary metabolites, in addition to their role in osmoregulation (89). This is consistent with results for *Rhodococcus biphenylivorans* grown on phenol compared to glucose (27). The level of L-histidinol, a histidine biosynthesis metabolite, was also higher in the DBT culture (Tables S3 through S5). Increased biosynthesis of glutamate and histidine could be important for the DBT culture to synthesize the low-molecular-weight thiol ergothioneine and 5-methyltetrahydropteroyltri-L-glutamate, the cofactor of the methionine biosynthesis enzyme MetE. Both ergothioneine and MetE are enriched under biodesulfurization conditions (19). Consistent with these findings, dihydrofolate synthase/folylpolyglutamate synthase, which catalyzes successive addition of L-glutamate to tetrahydrofolate, was significantly more abundant in the DBT culture (Tables S1 and S2). Serine biosynthesis enzymes (3-phosphoglycerate dehydrogenase and phosphoserine phosphatase) and serineacetyltransferase (CysE) were significantly more abundant in the DBT culture (Tables S1 and S2), accounting for the higher content of *O*-acetyl-L-serine that we reported earlier and provide further evidence for the role of direct sulfhydrylation in cysteine biosynthesis in the biodesulfurizing culture (19).

Enzymes of valine/leucine/isoleucine degradation and glycine/serine/threonine turnover were significantly upregulated in the DBT culture, which could enable a better supply of energy, reducing equivalents, and anabolic precursors (90) (Fig. 6). Perhaps the significantly higher glycine content in the DBT culture is due to simultaneous upshift of sarcosine oxidase abundance and depletion of a glycine oxidase. The latter produces

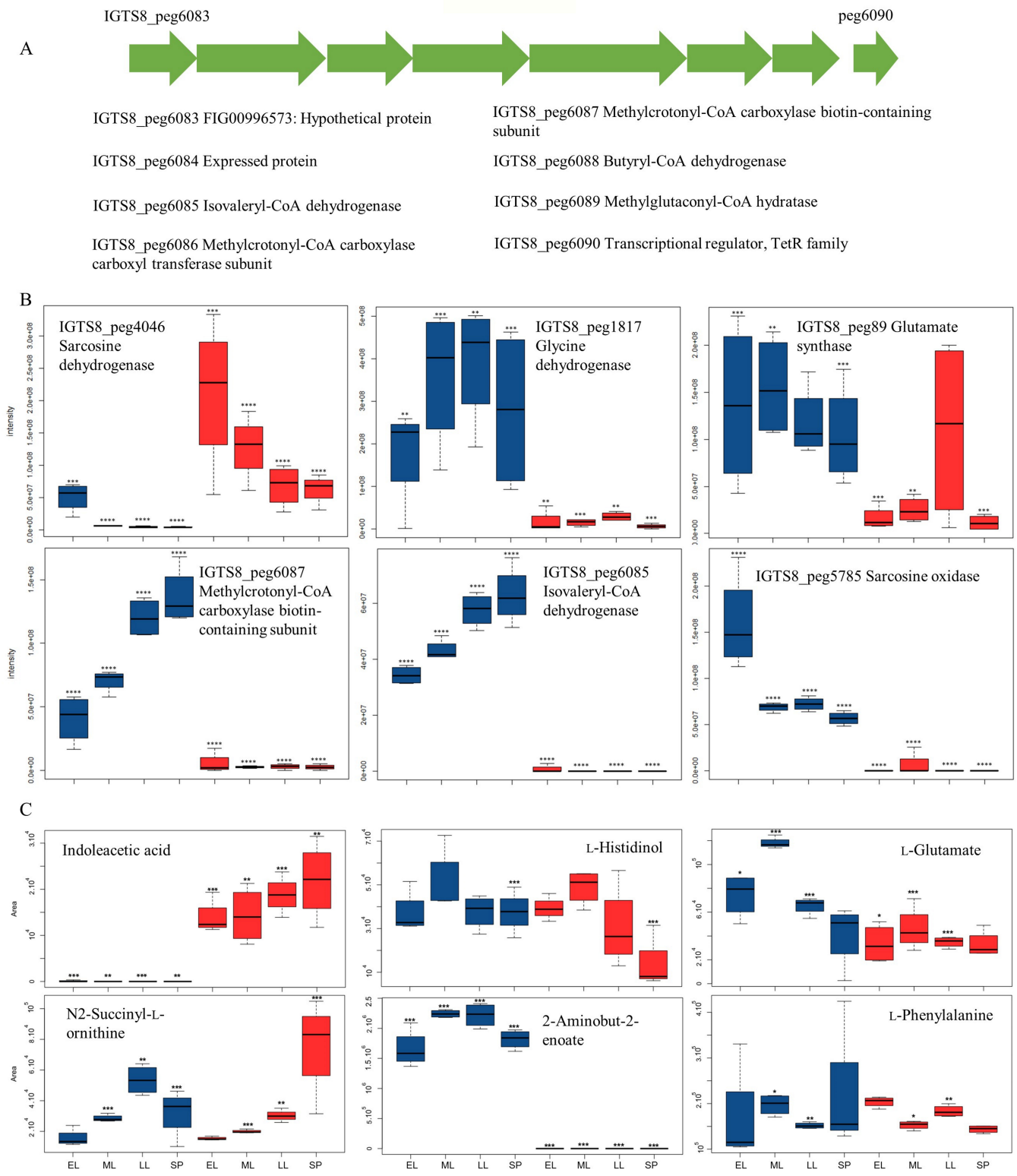

FIG 6 (A) A gene cluster encoding proteins of valine/leucine/isoleucine degradation. (B) Boxplots of the label-free quantification (LFQ) values showing the abundance of the profile of amino acid metabolism proteins and (C) metabolites in the dibenzothiophene (DBT, in blue) and inorganic sulfate ($MgSO_4$, IS, in red) cultures. The growth phases are abbreviated as EL (early-log), ML (mid-log), LL (late-log), and SP (stationary phase). Significance is attested by a Limma moderated *t*-test as follows: no * $P > 0.05$, *$P \leq 0.05$, **$P \leq 0.01$, ***$P \leq 0.001$, ****$P \leq 0.0001$.

H_2O_2, thus its decreased abundance could mitigate oxidative stress. Increased glycine cleavage in the DBT culture may not only mitigate its inhibitory effect on growth and cell wall biosynthesis (91) but also supply additional NADH, and thus energy, for desulfurization (92). In addition, glycine cleavage produces an activated methylene group in the form of 5, 10-methylenetetrahydrofolate which is used in the synthesis of purines, pyrimidines, methionine, and *S*-adenosylmethionine (93).

Nucleotide metabolism and genetic information processing

Proteins of DNA replication, transcriptional regulation, purine and pyrimidine metabolism, DNA repair, biosynthesis of modified nucleotides (pseudouridine, queuosine), environmental information processing, chromosome partitioning, RNA processing, ribosome biogenesis, as well as cAMP receptor protein were all differentially produced *R. qingshengii* IGTS8 depending on the sulfur source (Fig. 7; Tables S1 and S2). In line with the proteomics data, the metabolome revealed 16 differentially abundant metabolites, mainly related to purine and pyrimidine nucleotide metabolism. The majority of these metabolites were less abundant in the DBT cultures (Tables S3 through S5). For instance, the sulfate culture had a higher content of 7-aminoethyl-7-deazaguanine, an intermediate of the biosynthesis of the modified nucleotide queuosine from *S*-adenosylmethionine present in certain tRNAs (transfer ribonucleic acid). Most of the identified transcriptional regulators were more abundant in the DBT culture. The differential expression of many transcriptional regulators, including two-component systems, sRNA (small ribonucleic acid), and RNases could be a mechanism of natural adaptation of the bacterium to the low availability of sulfur in the form of DBT. Alternatively, it suggests a need in the biodesulfurizing culture to control and reorganize its physiology and metabolism as a part of its global stress response (94, 95).

MprAB, which induces the production of the serine protease chaperone PepD, may serve as an example (Fig. 7A and B). In *Mycobacterium tuberculosi*s, PepD binds a 35-kDa antigen whose cleavage helps maintain cell wall homeostasis and regulate stress response pathways (96, 97). Moreover, MprAB directly regulates the expression of the alternative sigma factors SigB and SigE (97). In addition to a previously reported putative extracytoplasmic function sigma factor SigE (19), we found here that SigB was also more abundant under biodesulfurization conditions (Fig. 7B; Tables S1 and S2). Both allow the adaptation response of bacteria to environmental stimuli causing starvation, cell envelope stress, and oxidative stress (73, 98–100).

A global and fast stress response requires a higher fidelity and efficiency of the protein biosynthesis machinery. This can be inferred from the higher abundance of proteins involved in tRNA modification and ribosome biogenesis in the DBT culture, for example, formyltransferase, rRNA methyltransferase, tRNA-i(6) A37 methylthiotransferase, and proteins of pseudouridine and queuosine biosynthesis (Fig. 7B; Tables S1 and S2). Translational fidelity can have an impact on the proteome, thus contributing to responses to stressful conditions (101, 102). Post-transcriptional modifications affect stability, enhance decoding efficiency, increase ribosomal binding affinity, and promote correct tRNA and mRNA translocation through the ribosome (103–105). Queuosine deficiency in the anticodons of tRNAs reduce cell viability during the stationary phase (106), renders cells sensitive to oxidative stress, and affects metal homeostasis (102, 107). The lower abundance of the queuosine precursor, 7-aminomethyl-7-deazaguanine (preQ1) in the DBT culture could be due to higher consumption for queuosine biosynthesis. In addition, the higher abundance of several RNases in the DBT culture, such as RNase P and RNase III, suggests a role in RNA processing and ribosome biogenesis and as coordinators of bacterial stress response. Deletion of RNase-encoding genes in *Pseudomonas putida* reduced the growth rate and increased its sensitivity to inhibitory chemicals and oxidative and temperature stress (95). Further discussion on RNA modification is included in the Supplementary Material.

The significantly higher abundance of adenylate cyclase and cyclic AMP receptor protein (CRP) in the DBT culture (Tables S1 and S2) suggests a role of the signaling

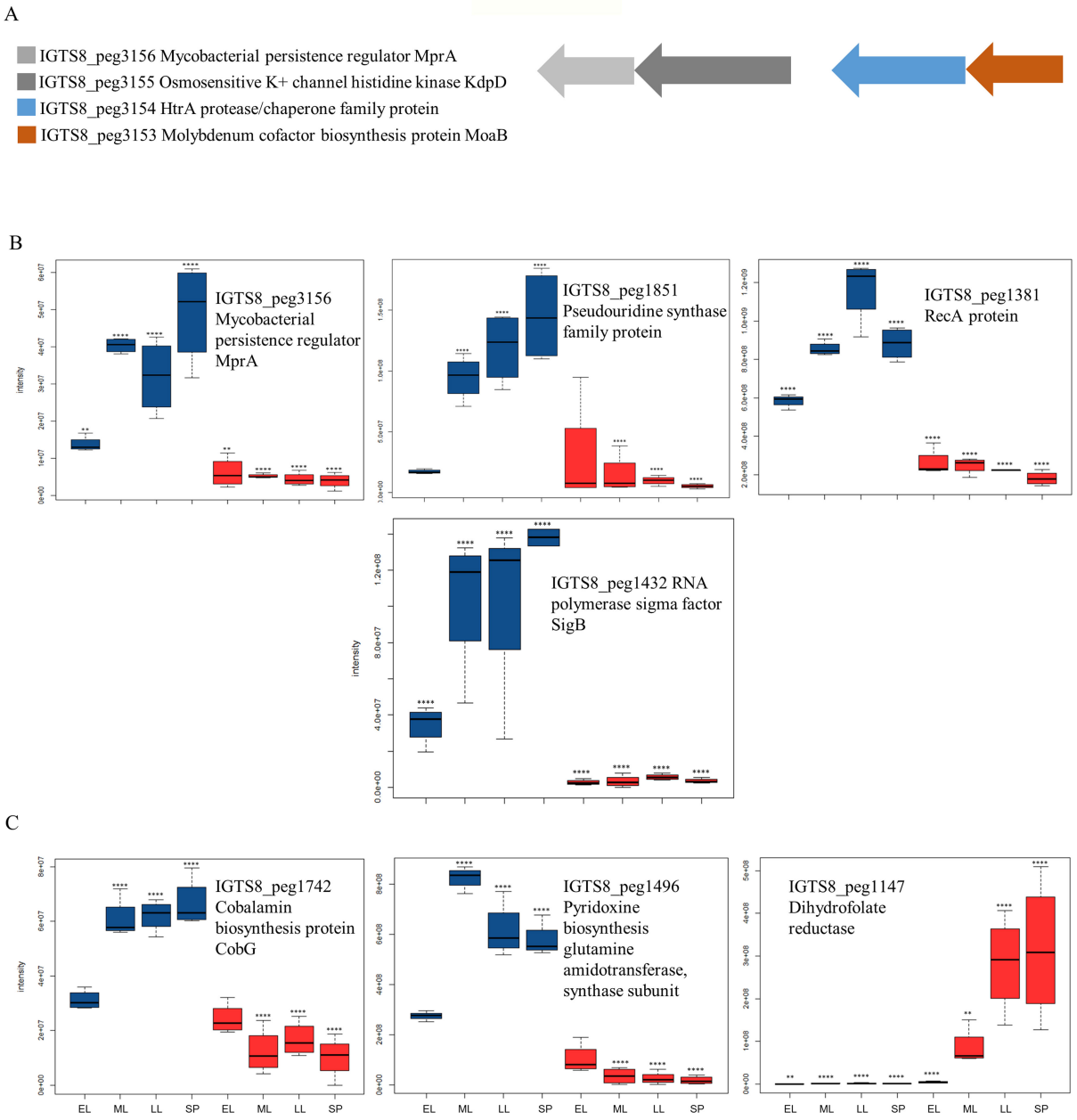

FIG 7 (A) Gene cluster encoding the mycobacterial persistence regulator. (B) Boxplots of the label-free quantification (LFQ) values showing the abundance profile of proteins involved in genetic information processing, and (C) vitamin and cofactor metabolism in the dibenzothiophene (DBT, in blue) and inorganic sulfate ($MgSO_4$, IS, in red) cultures. The growth phases are abbreviated as EL (early-log), ML (mid-log), LL (late-log), and SP (stationary phase). Significance is attested by a Limma moderated *t*-test as follows: no * $P > 0.05$, *$P \leq 0.05$, **$P \leq 0.01$, ***$P \leq 0.001$, ****$P \leq 0.0001$.

molecule cAMP in the regulation of gene expression. Cyclic AMP itself was less abundant in the DBT culture (Tables S3 and S4), probably because it was bound to CRP which regulates processes such as the TCA cycle, stress response, osmoregulation, nitrogen assimilation (108), and triacylglycerol biosynthesis (109). We searched the IGTS8 genome for CRP consensus-binding sites (5′-GTGANNTGNGTCAC-3′) (109) using online Find Individual Motif Occurrences Version 5.5.0 (19, 110, 111) and found 203 hits (Tables S6 through S8) in the proximity of genes encoding many of the differentially produced proteins involved in the following: mycofactocin biosynthesis, TCA cycle, carbohydrate metabolism, iron transport, the stringent response, nitrosative stress, mycobacterial persistence, cell cycle, MCE proteins, as well as amino acid and nucleotide metabolism. In

addition, genes encoding proteins of biosynthesis of biotin and the low-molecular-weight thiols mycothiol and ergothioneine, which we found previously to be upregulated in the DBT culture (19) are located close to putative CRP-binding sites.

Metabolism of vitamins and cofactors

Biodesulfurization was accompanied by changes in the production of vitamins and cofactors such as cobalamin, riboflavin, vitamin B6, or coenzyme F420 (Fig. 7C; Tables S2 and S3). These results reflected changes in the abundance of the respective biosynthetic enzymes such as glutamine amidotransferase involved in B6 production via the pyridoxal 5′-phosphate synthase complex, YggS mediating pyridoxal 5′-phosphate homeostasis (112, 113), or enzymes of the biosynthesis of cobalamin, which is required for the proper functioning of ethanolamine ammonia lyase (114).

Energy conservation

Many proteins with a role in energy conservation were enriched in the DBT culture (Tables S1 and S2) including ATP synthase F0 sector subunit c, cytochrome d-ubiquinol oxidase subunit II, flavodoxin, and UDP-galactose-lipid carrier transferase. The higher abundance of these proteins likely reflects the higher energy demand of the DBT culture, due to the upregulated proteins and stress-related products (19) and the need to maintain cellular viability and resist stress-related damage (115).

Morphological and ultrastructural changes in the biodesulfurizing culture

Morphological and ultrastructural changes in bacteria are common responses to various stressors (73). The DBT-grown culture was dominated by cells that appeared shorter and broader than the $MgSO_4$-grown cells, particularly during the early- and mid-log phases. Moreover, the DBT culture was characterized by cells having multiple division septa and irregular shapes, both of which were not observed in the $MgSO_4$ cultures (Fig. 8). This is consistent with the differential synthesis of cell cycle proteins, indicating reductive division and cell cycle perturbations (85) (Tables S1 and S2). A similar response to carbon starvation was reported for *Rhodococcus jostii* RHA1 (25). During the early-log phase, the cells contained electron-dense (dark) areas or inclusion bodies, probably polyphosphates (85, 116) or oligobodies (48), which were relatively more abundant on DBT. Differently shaped electron-transparent inclusions possibly composed of triacylglycerols (116–118) were more abundant during growth on $MgSO_4$ (Further discussion of triacylglycerol production can be found in the Supplementary Material.). Similar inclusion bodies were observed in biodesulfurizing *Gordonia* sp. SC-10 but were not found in the absence of DBT or diesel and, therefore, postulated to represent accumulation of the organosulfur substrates (82). A number of cells from the mid-log phase of the DBT culture revealed spherical extensions or vesicle-like structures protruding from the cell surface. These cell surface–associated vesicles are reminiscent of the outer membrane vesicles produced by Gram-negative bacteria on exposure to xenobiotics, osmotic stress, and heat shock (119, 120). In Gram-negative bacteria, these vesicles are composed of proteins and fatty acids and are one of the stress responses that lead to increased cell surface hydrophobicity and promote biofilm formation (119, 120). How they could be produced in Gram-positive bacteria and their role in the desulfurizing culture remain to be unveiled.

Other stress responses of the biodesulfurizing *R. qingshengii* IGTS8

A general stress response of *R. qingshengii* IGTS8 under biodesulfurization conditions was evident from the increased production of a large arsenal of stress-related proteins (32 proteins). Most of these proteins (85%) were significantly overrepresented in the biodesulfurizing culture (73, 121). The most significantly enriched proteins include those involved in transcriptional regulation (SigB, stress-associated sigma factor), biosynthesis of osmoprotectants, and the alarmone of the stringent response (ppGpp), oxidative

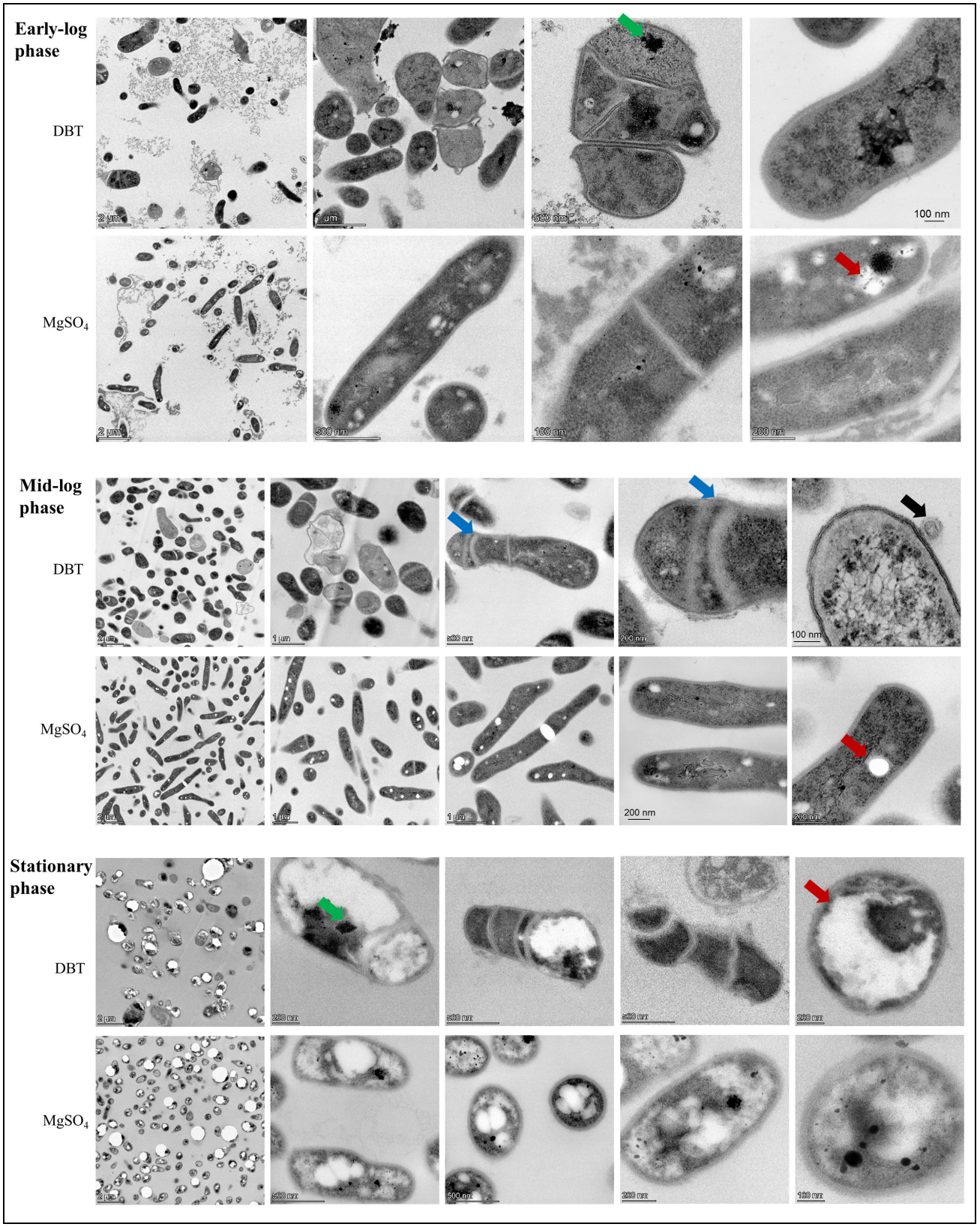

FIG 8 TEM images of the DBT and $MgSO_4$ cultures of *R. qingshengii* IGTS8 at different growth phases. Green arrows: electron-dense inclusions, red arrows: electron-transparent inclusions, blue arrows: multiple division septa, and black arrow: cell-surface-associated vesicles or extensions.

stress, Ter stress response, peptide transport, cell division under stress (cell filamentation protein, fic), in addition to several chaperones (Fig. 9; Tables S1 and S2).

Higher production of the osmoprotectant ectoine in the DBT culture was confirmed by its accumulation (up to 39-fold), consistent with the upregulation of the ectoine biosynthesis enzymes (Fig. 9; Tables S1 and S2). Moreover, 2-(α-D-mannosyl)-D-glycerate (another compatible solute) was much more abundant in the DBT cultures (up to 17-fold) (Fig. 9). Although this response has not been reported for biodesulfurizing or sulfate-deprived cultures, and there was no osmotic stress in the DBT culture, these compounds could protect proteins from aggregation under different stress conditions, such as heat, desiccation, freezing, and thawing, thus highlighting overlap of stress responses (73, 122).

The strong upregulation of dipeptide/oligopeptide transport proteins in the DBT culture (Tables S1 and S2) may reflect attempts to scavenge sulfur from peptides containing sulfur amino acids and may constitute a sulfate starvation-specific response as reported in *Brevibacterium aurantiacum* (123). Alternatively, it could be a general nutrient starvation response (124). The proteomics data provide clues to the induction of the stringent response in the DBT culture. Since the stringent response comes into play under nutrient starvation (125), it can be postulated that lack of sulfate and potential glucose-induced carbon limitation stress in the biodesulfurizing culture were, at least partially, the triggers of the stringent response.

It is worth noting that genes encoding many of the differentially produced proteins are grouped within the IGTS8_peg6050-6150 segment of the genome, including proteins of the MCE family (IGTS8_peg6054-6062), valine/leucine/isoleucine

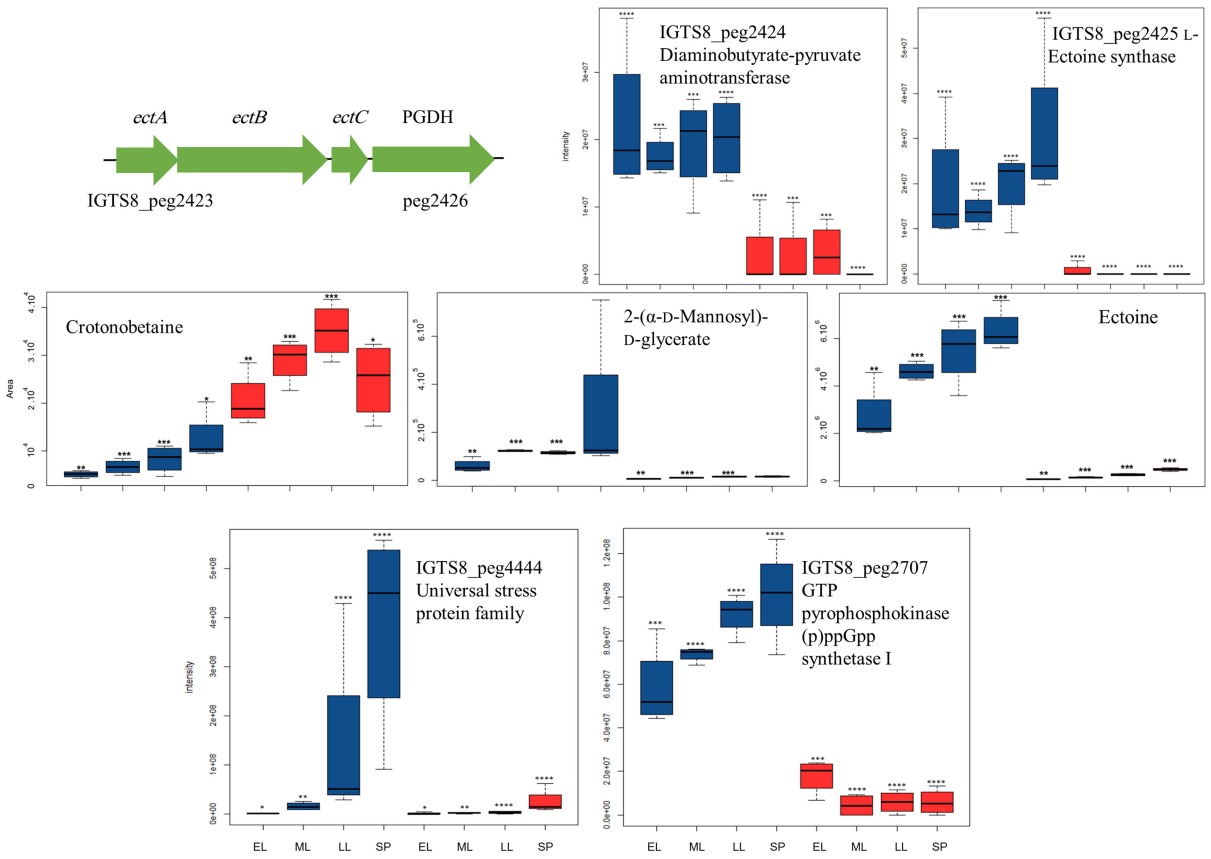

FIG 9 A gene cluster encoding ectoine biosynthesis proteins and boxplots of the label-free quantification (LFQ) values showing the abundance profile of some ectoine biosynthesis and stress response proteins, as well as osmoprotectants in the dibenzothiophene (DBT, in blue) and inorganic sulfate ($MgSO_4$, IS, in red) cultures. The growth phases are abbreviated as EL (early-log), ML (mid-log), LL (late-log), and SP (stationary phase). Significance is attested by a Limma moderated *t*-test as follows: no * $P > 0.05$, *$P \leq 0.05$, **$P \leq 0.01$, ***$P \leq 0.001$, ****$P \leq 0.0001$. PGDH: phosphoglycerate dehydrogenase.

degradation (IGTS8_peg6083-6090), MoxR/CoxE/ThcE (IGTS8_peg6110-6112), mycofactocin (IGTS8_peg6130-6144), and ethanolamine utilization (IGTS8_peg6146-6148), suggesting this segment as a potential active genomic island.

Conclusions

Contrary to earlier assumptions, biodesulfurization in *R. qingshengii* IGTS8 causes a far-reaching stress response that exceeds the central desulfurization pathway and even sulfur assimilation. Extensive metabolic reorganization and physiological responses reflect the complexity of the biodesulfurization phenotype and highlight the importance of a thorough and global understanding of the physiology and metabolism of fuel-biodesulfurizing microbes. Generally, the observed biodesulfurization-induced responses mimic those known to occur under nutrient starvation, osmotic stress, xenobiotic stress, and heat stress, suggesting an overlap of stress response pathways which are orchestrated to ensure the protection and survival of the culture and to optimize resource management. The notion that glucose is not the most preferred carbon source for *R. qingshengii* IGTS8 during biodesulfurization raises the possibility that some of the detected physiological and metabolic adaptations may be driven by the specific combination of glucose and DBT. Due to our experimental design and the known overlap of stress response pathways, it was not possible to determine which responses were specifically triggered by potential glucose-related stresses. Despite this limitation, our findings not only pave the way toward a better understanding of the physiology and metabolism of fuel-biodesulfurizing bacteria but also empower current and future efforts to promote biodesulfurization catalytic efficiency. This could be approached via directed evolution and metabolic engineering endeavors that enable better protection of biodesulfurizing cells and improve the metabolic flux in pathways that could ultimately lead to higher sulfur utilization rates. Circumventing the slow growth via manipulating the cell cycle machinery and the resuscitation factors constitutes a potential intervention. In particular, the role of mycofactocin and the glyoxylate shunt, the importance of oligotrophy, lipid metabolism, as well as cell surface modifications are worth investigating.

ACKNOWLEDGMENTS

This study was funded by the Kuwait Foundation for the Advancement of Sciences (Grant no. P215-42SL-02). Proteomics experiments were supported by the French Proteomic Infrastructure (ProFI FR2048, ANR-10-INBS-08-03).

The authors declare that they have no competing interests.

AUTHOR AFFILIATIONS

[1]Institut de Biologie Moléculaire des Plantes, CNRS, Université de Strasbourg, Strasbourg, France
[2]Laboratoire de Spectrométrie de Masse BioOrganique, CNRS, Université de Strasbourg, IPHC UMR 7178, Infrastructure Nationale de Protéomique ProFI FR2048, Strasbourg, France
[3]Département mécanique, ICube Laboratoire des sciences de l'ingénieur, de l'informatique et de l'imagerie, UNISTRA/CNRS/ENGEES/INSA, Strasbourg, France
[4]Institut für Mikrobiologie & Biotechnologie, Rheinische Friedrich-Wilhelms-Universität Bonn, Bonn, Germany
[5]Environmental Biotechnology Program, Life Sciences Department, College of Graduate Studies, Arabian Gulf University, Manama, Bahrain
[6]Faculty of Health and Life Sciences, Northumbria University, Newcastle upon Tyne, United Kingdom
[7]Department of Biological Sciences, Faculty of Science, Kuwait University, Kuwait City, Kuwait

AUTHOR ORCIDs

Wael Ismail http://orcid.org/0000-0002-3027-928X

FUNDING

Funder	Grant(s)	Author(s)
Kuwait Foundation for the Advancement of Sciences (KFAS)	P215-42SL-02	Wael Ismail

AUTHOR CONTRIBUTIONS

Julie Zumsteg, Data curation, Formal analysis, Writing – review and editing | Aurélie Hirschler, Data curation, Formal analysis, Investigation, Methodology, Writing – review and editing | Christine Carapito, Data curation, Formal analysis, Supervision, Writing – review and editing | Loïc Maurer, Data curation, Formal analysis, Writing – review and editing | Claire Villette, Methodology, Writing – review and editing | Dimitri Heintz, Methodology, Supervision, Writing – review and editing | Christiane Dahl, Formal analysis, Writing – review and editing | Ashraf El Nayal, Methodology, Writing – review and editing | Vartul Sangal, Formal analysis, Writing – review and editing | Huda Mahmoud, Conceptualization, Funding acquisition, Project administration, Writing – review and editing | Alain Van Dorsselaer, Supervision, Writing – review and editing | Wael Ismail, Conceptualization, Formal analysis, Funding acquisition, Project administration, Supervision, Writing – original draft, Writing – review and editing

DATA AVAILABILITY

Data that support the findings of this study are openly available in the ProteomeXchange Consortium via the PRIDE partner repository, reference no. PXD021362.

ADDITIONAL FILES

The following material is available online.

Supplemental Material

Supplemental material (AEM00826-23-s0001.docx). Fig. S1 to S18, additional experimental details, and supplemental results and discussion.
Table S1 (AEM00826-23-s0002.xlsx). Differential proteomic analysis.
Table S2 (AEM00826-23-s0003.docx). Functional categories of proteins.
Table S3 (AEM00826-23-s0004.docx). Functional categories of metabolites.
Table S4 (AEM00826-23-s0005.xlsx). Differential analysis of the metabolites detected by LC/MS.
Table S5 (AEM00826-23-s0006.xlsx). Differential analysis of the metabolites detected by GC-MS.
Table S6 (AEM00826-23-s0007.xlsx). CRP consensus binding sites identified in the genome of the IGTS8 strain.
Table S7 (AEM00826-23-s0008.xlsx). Genes having CRP binding sites 500 bp upstream or downstream.
Table S8 (AEM00826-23-s0009.xlsx). Genes having CRP binding sites >500-1000 bp upstream or downstream.

REFERENCES

1. Kilbane JJ. 1990. Sulfur-specific microbial metabolism of organic compounds. Resour Conserv Recycl 3:69–79. https://doi.org/10.1016/0921-3449(90)90046-7
2. Kilbane JJ, Bielaga B. 1990. Toward sulfur-free fuels. Chemtech 20:747–751.
3. Denome SA, Olson ES, Young KD. 1993. Identification and cloning of genes involved in specific desulfurization of dibenzothiophene by *Rhodococcus* sp. strain IGTS8. Appl Environ Microbiol 59:2837–2843. https://doi.org/10.1128/aem.59.9.2837-2843.1993
4. Kilbane JJ. 2006. Microbial biocatalyst developments to upgrade fossil fuels. Curr Opin Biotechnol 17:305–314. https://doi.org/10.1016/j.copbio.2006.04.005
5. Chen S, Zhao C, Liu Q, Zang M, Liu C, Zhang Y. 2018. Thermophilic biodesulfurization and its application in oil desulfurization. Appl

Microbiol Biotechnol 102:9089–9103. https://doi.org/10.1007/s00253-018-9342-5
6. Paixão SM, Silva TP, Arez BF, Alves L. 2020. Advances in the reduction of the costs inherent to fossil fuel biodesulfurization towards its potential industrial applications, p 235–283. In Saleh TA (ed), Nanocomposites for the desulfurization of fuels, IGI global. https://doi.org/10.4018/978-1-7998-2146-5
7. Thompson D, Cognat V, Goodfellow M, Koechler S, Heintz D, Carapito C, Van Dorsselaer A, Mahmoud H, Sangal V, Ismail W. 2020. Phylogenomic classification and biosynthetic potential of the fossil fuel-biodesulfurizing *Rhodococcus* strain IGTS8. Front Microbiol 11:1417. https://doi.org/10.3389/fmicb.2020.01417
8. Martínez I, Mohamed M-S, Rozas D, García JL, Díaz E. 2016. Engineering synthetic bacterial consortia for enhanced desulfurization and revalorization of oil sulfur compounds. Metab Eng 35:46–54. https://doi.org/10.1016/j.ymben.2016.01.005
9. Martínez I, El-Said Mohamed M, Santos VE, García JL, García-Ochoa F, Díaz E. 2017. Metabolic and process engineering for biodesulfurization in gram-negative bacteria. J Biotechnol 262:47–55. https://doi.org/10.1016/j.jbiotec.2017.09.004
10. Martínez I, Mohamed M-S, García JL, Díaz E. 2022. Enhancing biodesulfurization by engineering a synthetic dibenzothiophene mineralization pathway. Front Microbiol 13:987084. https://doi.org/10.3389/fmicb.2022.987084
11. Kilbane JJ. 2017. Biodesulfurization: how to make it work? Arab J Sci Eng 42:1–9. https://doi.org/10.1007/s13369-016-2269-1
12. Li L, Liao Y, Luo Y, Zhang G, Liao X, Zhang W, Zheng S, Han S, Lin Y, Liang S. 2019. Improved efficiency of the desulfurization of oil sulfur compounds in *Escherichia coli* using a combination of desensitization engineering and DszC overexpression. ACS Synth Biol 8:1441–1451. https://doi.org/10.1021/acssynbio.9b00126
13. Parveen S, Akhtar N, Ghauri MA, Akhtar K. 2020. Conventional genetic manipulation of desulfurizing bacteria and prospects of using CRISPR-Cas systems for enhanced desulfurization activity. Crit Rev Microbiol 46:300–320. https://doi.org/10.1080/1040841X.2020.1772195
14. Martzoukou O, Amillis S, Glekas PD, Breyanni D, Avgeris M, Scorilas A, Kekos D, Pachnos M, Mavridis G, Mamma D, Hatzinikolaou DG. 2023. Advancing desulfurization in the model biocatalyst *Rhodococcus qingshengii* IGTS8 via an *in locus* combinatorial approach. Appl Environ Microbiol 89:e0197022. https://doi.org/10.1128/aem.01970-22
15. Kilbane JJ, Stark B. 2016. Biodesulfurization: a model system for microbial physiology research. World J Microbiol Biotechnol 32:137. https://doi.org/10.1007/s11274-016-2084-6
16. Aggarwal S, Karimi IA, Kilbane Ii JJ, Lee DY. 2012. Roles of sulfite oxidoreductase and sulfite reductase in improving desulfurization by *Rhodococcus erythropolis*. Mol Biosyst 8:2724–2732. https://doi.org/10.1039/c2mb25127b
17. Aggarwal S, Karimi IA, Ivan GR. 2013. *In silico* modeling and evaluation of *Gordonia alkanivorans* for biodesulfurization. Mol Biosyst 9:2530–2540. https://doi.org/10.1039/c3mb70132h
18. Wang J, Butler RR, Wu F, Pombert J-F, Kilbane JJ, Stark BC. 2017. Enhancement of microbial biodesulfurization via genetic engineering and adaptive evolution. PLoS One 12:e0168833. https://doi.org/10.1371/journal.pone.0168833
19. Hirschler A, Carapito C, Maurer L, Zumsteg J, Villette C, Heintz D, Dahl C, Al-Nayal A, Sangal V, Mahmoud H, Van Dorsselaer A, Ismail W. 2021. Biodesulfurization induces reprogramming of sulfur metabolism in *Rhodococcus qingshengii* IGTS8: proteomics and untargeted metabolomics. Microbiol Spectr 9:e0069221. https://doi.org/10.1128/Spectrum.00692-21
20. Abbad-Andaloussi S, Lagnel C, Warzywoda M, Monot F. 2003. Multicriteria comparison of resting cell activities of bacterial strains selected for biodesulfurization of petroleum compounds. Enzyme Microb Technol 32:446–454. https://doi.org/10.1016/S0141-0229(02)00320-4
21. Noda K-I, Watanabe K, Maruhashi K. 2003. Isolation of a recombinant desulfurizing 4,6-diproply dibenzothiophene in n-tetradecane. J Biosci Bioeng 95:354–360. https://doi.org/10.1016/s1389-1723(03)80067-1
22. Tanaka Y, Yoshikawa O, Maruhashi K, Kurane R. 2002. The cbs mutant strain of *Rhodococcus erythropolis* KA2-5-1 expresses high levels of Dsz enzymes in the presence of sulfate. Arch Microbiol 178:351–357. https://doi.org/10.1007/s00203-002-0466-7
23. Dorado-Morales P, Martínez I, Rivero-Buceta V, Díaz E, Bähre H, Lasa I, Solano C. 2021. Elevated c-di-GMP levels promote biofilm formation and biodesulfurization capacity of *Rhodococcus erythropolis*. Microb Biotechnol 14:923–937. https://doi.org/10.1111/1751-7915.13689
24. Tralau T, Vuilleumier S, Thibault C, Campbell BJ, Hart CA, Kertesz MA. 2007. Transcriptomic analysis of the sulfate starvation response of *Pseudomonas aeruginosa*. J Bacteriol 189:6743–6750. https://doi.org/10.1128/JB.00889-07
25. Patrauchan MA, Miyazawa D, LeBlanc JC, Aiga C, Florizone C, Dosanjh M, Davies J, Eltis LD, Mohn WW. 2012. Proteomic analysis of survival of *Rhodococcus jostii* RHA1 during carbon starvation. Appl Environ Microbiol 78:6714–6725. https://doi.org/10.1128/AEM.01293-12
26. Männle D, McKinnie SMK, Mantri SS, Steinke K, Lu Z, Moore BS, Ziemert N, Kaysser L. 2020. Comparative genomics and metabolomics in the genus *Nocardia*. mSystems 5:e00125-20. https://doi.org/10.1128/mSystems.00125-20
27. Xie X, Liu J, Jiang Z, Li H, Ye M, Pan H, Zhu J, Song H. 2021. The conversion of the nutrient condition alter the phenol degradation pathway by *Rhodococcus biphenylivorans* B403: a comparative transcriptomic and proteomic approach. Environ Sci Pollut Res Int 28:56152–56163. https://doi.org/10.1007/s11356-021-14374-8
28. Wang W, Ma T, Lian K, Zhang Y, Tian H, Ji K, Li G. 2013. Genetic analysis of benzothiophene biodesulfurization pathway of *Gordonia terrae* strain C-6. PLoS One 8:e84386. https://doi.org/10.1371/journal.pone.0084386
29. Peng C, Huang D, Shi Y, Zhang B, Sun L, Li M, Deng X, Wang W. 2019. Comparative transcriptomic analysis revealed the key pathways responsible for organic sulfur removal by thermophilic bacterium *Geobacillus thermoglucosidasius* W-2. Sci Total Environ 676:639–650. https://doi.org/10.1016/j.scitotenv.2019.04.328
30. Kertesz MA, Wietek C. 2001. Desulfurization and desulfonation: applications of sulfur-controlled gene expression in bacteria. Appl Microbiol Biotechnol 57:460–466. https://doi.org/10.1007/-s002530100800
31. Martzoukou O, Glekas PD, Avgeris M, Mamma D, Scorilas A, Kekos D, Amillis S, Hatzinikolaou DG. 2022. Interplay between sulfur assimilation and biodesulfurization activity in *Rhodococcus qingshengii* IGTS8: insights into a regulatory role of the reverse transsulfuration pathway. mBio 13:e0075422. https://doi.org/10.1128/mbio.00754-22
32. Tyanova S, Temu T, Cox J. 2016. The MaxQuant computational platform for mass spectrometry-based shotgun proteomics. Nat Protoc 11:2301–2319. https://doi.org/10.1038/nprot.2016.136
33. Wieczorek S, Combes F, Lazar C, Giai Gianetto Q, Gatto L, Dorffer A, Hesse A-M, Couté Y, Ferro M, Bruley C, Burger T. 2017. DAPAR & ProStaR: software to perform statistical analyses in quantitative discovery proteomics. Bioinformatics 33:135–136. https://doi.org/10.1093/bioinformatics/btw580
34. Deutsch EW, Csordas A, Sun Z, Jarnuczak A, Perez-Riverol Y, Ternent T, Campbell DS, Bernal-Llinares M, Okuda S, Kawano S, Moritz RL, Carver JJ, Wang M, Ishihama Y, Bandeira N, Hermjakob H, Vizcaíno JA. 2017. The ProteomeXchange consortium in 2017: supporting the cultural change in proteomics public data deposition. Nucleic Acids Res 45:D1100–D1106. https://doi.org/10.1093/nar/gkw936
35. Pearson WR. 1996. Effective protein sequence comparison. Methods Enzymol 266:227–258. https://doi.org/10.1016/s0076-6879(96)66017-0
36. Huang DW, Sherman BT, Lempicki RA. 2009. Bioinformatics enrichment tools: paths toward the comprehensive functional analysis of large gene lists. Nucleic Acids Res 37:1–13. https://doi.org/10.1093/nar/gkn923
37. Huang DW, Sherman BT, Lempicki RA. 2009. Systematic and integrative analysis of large gene lists using DAVID bioinformatics resources. Nat Protoc 4:44–57. https://doi.org/10.1038/nprot.2008.211
38. Awadh M, Mahmoud H, Abed RMM, El Nayal AM, Abotalib N, Ismail W. 2020. Diesel-born organosulfur compounds stimulate community restructuring in a diesel-biodesulfurizing consortium. Biotechnol Rep (Amst) 28:e00572. https://doi.org/10.1016/j.btre.2020.e00572
39. Hernández MA, Alvarez HM, Lanfranconi MP, Silva RA, Herrero OM, Villalba MS. 2019. Central metabolism of species of the genus *Rhodococcus*, p 61–85. In Alvarez H (ed), Biology of *Rhodococcus*. Microbiology monographs. Springer, Cham. https://doi.org/10.1007/978-3-030-11461-9

40. Tupa PR, Masuda H. 2018. Comparative proteomic analysis of propane metabolism in *Mycobacterium sp*. strain ENV421 and *Rhodococcus sp*. strain ENV425. J Mol Microbiol Biotechnol 28:107–115. https://doi.org/10.1159/000490494
41. Roell GW, Carr RR, Campbell T, Shang Z, Henson WR, Czajka JJ, Martín HG, Zhang F, Foston M, Dantas G, Moon TS, Tang YJ. 2019. A concerted systems biology analysis of phenol metabolism in *Rhodococcus opacus* PD630. Metab Eng 55:120–130. https://doi.org/10.1016/j.ymben.2019.06.013
42. Muñoz-Elías EJ, McKinney JD. 2005. *Mycobacterium tuberculosis* isocitrate lyases 1 and 2 are jointly required for *in vivo* growth and virulence. Nat Med 11:638–644. https://doi.org/10.1038/nm1252
43. Beste DJV, Bonde B, Hawkins N, Ward JL, Beale MH, Noack S, Nöh K, Kruger NJ, Ratcliffe RG, McFadden J. 2011. ^{13}C metabolic flux analysis identifies an unusual route for pyruvate Dissimilation in mycobacteria which requires isocitrate Lyase and carbon dioxide fixation. PLoS Pathog 7:e1002091. https://doi.org/10.1371/journal.ppat.1002091
44. Aggarwal S, Karimi IA, Lee DY. 2011. Reconstruction of a genome-scale metabolic network of *Rhodococcus erythropolis* for desulfurization studies. Mol Biosyst 7:3122–3131. https://doi.org/10.1039/c1mb05201b
45. Aggarwal S, Karimi IA, Lee DY. 2011. Flux-based analysis of sulfur metabolism in desulfurizing strains of *Rhodococcus erythropolis*. FEMS Microbiol Lett 315:115–121. https://doi.org/10.1111/j.1574-6968.2010.02179.x
46. Yan H, Kishimoto M, Omasa T, Katakura Y, Suga K, Okumura K, Yoshikawa O. 2000. Increase in desulfurization activity of *Rhodococcus erythropolis* KA2-5-1 using ethanol feeding. J Biosci Bioeng 89:361–366. https://doi.org/10.1016/s1389-1723(00)88959-8
47. Sauer U, Eikmanns BJ. 2005. The PEP-pyruvate-oxaloacetate node as the switch point for carbon flux distribution in bacteria. FEMS Microbiol Rev 29:765–794. https://doi.org/10.1016/j.femsre.2004.11.002
48. Yoshida N. 2019. Oligotrophic growth of *Rhodococcus*, p 87–101. In Alvarez H (ed), Biology of *Rhodococcus*. Microbiology monographs. Springer, Cham. https://doi.org/10.1007/978-3-030-11461-9
49. Wong KS, Houry WA. 2012. Novel structural and functional insights into the MoxR family of AAA+ ATPases. J Struct Biol 179:211–221. https://doi.org/10.1016/j.jsb.2012.03.010
50. Jessop M, Arragain B, Miras R, Fraudeau A, Huard K, Bacia-Verloop M, Catty P, Felix J, Malet H, Gutsche I. 2020. Structural insights into ATP hydrolysis by the MoxR ATPase RavA and the LdcI-RavA cage-like complex. Commun Biol 3:46. https://doi.org/10.1038/s42003-020-0772-0
51. Van Spanning RJ, Wansell CW, De Boer T, Hazelaar MJ, Anazawa H, Harms N, Oltmann LF, Stouthamer AH. 1991. Isolation and characterization of the *moxJ*, *moxG*, *moxI*, and *moxR* genes of *Paracoccus denitrificans*: inactivation of *moxJ*, *moxG*, and *moxR* and the resultant effect on methylotrophic growth. J Bacteriol 173:6948–6961. https://doi.org/10.1128/jb.173.21.6948-6961.1991
52. Pelzmann A, Ferner M, Gnida M, Meyer-Klaucke W, Maisel T, Meyer O. 2009. The CoxD protein of *Oligotropha carboxidovorans* is a predicted AAA+ ATPase chaperone involved in the biogenesis of the CO dehydrogenase [CuSmoO2] cluster. J Biol Chem 284:9578–9586. https://doi.org/10.1074/jbc.M805354200
53. Santiago B, Schübel U, Egelseer C, Meyer O. 1999. Sequence analysis, characterization and CO-specific transcription of the cox gene cluster on the megaplasmid pHCG3 of *Oligotropha carboxidovorans*. Gene 236:115–124. https://doi.org/10.1016/s0378-1119(99)00245-0
54. Pelzmann AM, Mickoleit F, Meyer O. 2014. Insights into the posttranslational assembly of the Mo-, S- and Cu-containing cluster in the active site of CO dehydrogenase of *Oligotropha carboxidovorans*. J Biol Inorg Chem 19:1399–1414. https://doi.org/10.1007/s00775-014-1201-y
55. Whittaker CA, Hynes RO. 2002. Distribution and evolution of von Willebrand/integrin A domains: widely dispersed domains with roles in cell adhesion and elsewhere. Mol Biol Cell 13:3369–3387. https://doi.org/10.1091/mbc.e02-05-0259
56. Nagy I, Schoofs G, Compernolle F, Proost P, Vanderleyden J, de Mot R. 1995. Degradation of the thiocarbamate herbicide EPTC (S-ethyl dipropylcarbamothioate) and biosafening by *Rhodococcus* sp. strain NI86/21 involve an inducible cytochrome P-450 system and aldehyde dehydrogenase. J Bacteriol 177:676–687. https://doi.org/10.1128/jb.177.3.676-687.1995
57. Ohhata N, Yoshida N, Egami H, Katsuragi T, Tani Y, Takagi H. 2007. An extremely oligotrophic bacterium, *Rhodococcus erythropolis* N9T-4, isolated from crude oil. J Bacteriol 189:6824–6831. https://doi.org/10.1128/JB.00872-07
58. Ikegaya R, Shintani M, Kimbara K, Fakuda M, Yoshida N. 2020. Identification of a transcriptional regulator for oligotrophy-responsive promoter in *Rhodococcus erythropolis* N9T-4. Biosci Biotechnol Biochem 84:865–868. https://doi.org/10.1080/09168451.2019.1709792
59. Misset-Smits M, van Ophem PW, Sakuda S, Duine JA. 1997. Mycothiol, 1-O-(2'-[*N*-acetyl-L-cysteinyl]amido-2'-deoxy-alpha-D-glucopyranosyl)-D-*myo*-inositol, is the factor of NAD/factor-dependent formaldehyde dehydrogenase. FEBS Lett 409:221–222. https://doi.org/10.1016/s0014-5793(97)00510-3
60. Yoshida N, Hayasaki T, Takagi H. 2011. Gene expression analysis of methylotrophic oxidoreductases involved in the oligotrophic growth of *Rhodococcus erythropolis* N9T-4. Biosci Biotechnol Biochem 75:123–127. https://doi.org/10.1271/bbb.100700
61. Yano T, Yoshida N, Yu F, Wakamatsu M, Takagi H. 2015. The glyoxylate shunt is essential for CO_2-requiring oligotrophic growth of *Rhodococcus erythropolis* N9T-4. Appl Microbiol Biotechnol 99:5627–5637. https://doi.org/10.1007/s00253-015-6500-x
62. Ikeda Y, Kishimoto M, Shintani M, Yoshida N. 2022. Oligotrophic gene expression in *Rhodococcus erythropolis* N9T-4 under various nutrient conditions. Microorganisms 10:1725. https://doi.org/10.3390/microorganisms10091725
63. Cordero PRF, Bayly K, Man Leung P, Huang C, Islam ZF, Schittenhelm RB, King GM, Greening C. 2019. Atmospheric carbon monoxide oxidation is a widespread mechanism supporting microbial survival. ISME J 13:2868–2881. https://doi.org/10.1038/s41396-019-0479-8
64. Alvarez HM, Herrero OM, Silva RA, Hernández MA, Lanfranconi MP, Villalba MS. 2019. Insights into the metabolism of oleaginous *Rhodococcus* spp. Appl Environ Microbiol 85:e00498-19. https://doi.org/10.1128/AEM.00498-19
65. Ayikpoe R, Govindarajan V, Latham JA. 2019. Occurrence, function, and biosynthesis of mycofactocin. Appl Microbiol Biotechnol 103:2903–2912. https://doi.org/10.1007/s00253-019-09684-4
66. Haft DH. 2011. Bioinformatic evidence for a widely distributed, ribosomally produced electron carrier precursor, its maturation proteins, and its nicotinoprotein redox partners. BMC Genomics 12:21. https://doi.org/10.1186/1471-2164-12-21
67. Nagy I, Verheijen S, De Schrijver A, Van Damme J, Proost P, Schoofs G, Vanderleyden J, De Mot R. 1995. Characterization of the *Rhodococcus* sp. NI86/21 gene encoding alcohol: *N,N'*-dimethyl-4-nitrosoaniline oxidoreductase inducible by atrazine and thiocarbamate herbicides. Arch Microbiol 163:439–446. https://doi.org/10.1007/BF00272133
68. Krishnamoorthy G, Kaiser P, Constant P, Abu Abed U, Schmid M, Frese CK, Brinkmann V, Daffé M, Kaufmann SHE. 2021. Role of premycofactocin synthase in growth, microaerophilic adaptation, and metabolism of *Mycobacterium tuberculosis*. mBio 12:e0166521. https://doi.org/10.1128/mBio.01665-21
69. Dubey AA, Wani SR, Jain V. 2018. Methylotrophy in mycobacteria: dissection of the methanol metabolism pathway in *Mycobacterium smegmatis*. J Bacteriol 200:e00288-18. https://doi.org/10.1128/JB.00288-18
70. Krishnamoorthy G, Kaiser P, Lozza L, Hahnke K, Mollenkopf H-J, Kaufmann SHE. 2019. Mycofactocin is associated with ethanol metabolism in mycobacteria. mBio 10:e00190-19. https://doi.org/10.1128/mBio.00190-19
71. Hassett JJ, Means JC, Banwart WL, Wood SG, Ali S, Khan A. 1980. Sorption of dibenzothiophene by soils and sediments. J Environ Qual 9:184–186. https://doi.org/10.2134/jeq1980.00472425000900020003x
72. Ju L-K, Kankipati P. 1998. Toxicity of dibenzothiophene to thermophile *Sulfolobus acidocaldarius* grown in sucrose medium. J Biotechnol 63:219–227. https://doi.org/10.1016/S0168-1656(98)00089-3
73. Pátek M, Grulich M, Nešvera J. 2021. Stress response in *Rhodococcus* strains. Biotechnol Adv 53:107698. https://doi.org/10.1016/j.biotechadv.2021.107698
74. Elbein AD, Pan YT, Pastuszak I, Carroll D. 2003. New insights on trehalose: a multifunctional molecule. Glycobiology 13:17R–27R. https://doi.org/10.1093/glycob/cwg047

75. Kuyukina MS, Ivshina IB. 2019. Production of trehalolipid biosurfactants by *Rhodococcus*, p 271–298. In Alvarez H (ed), Biology of *Rhodococcus*. Microbiology monographs. Springer, Cham. https://doi.org/10.1007/978-3-030-11461-9
76. Casali N, Riley LW. 2007. A phylogenomic analysis of the *Actinomycetales* mce operons. BMC Genomics 8:60. https://doi.org/10.1186/1471-2164-8-60
77. Mohn WW, van der Geize R, Stewart GR, Okamoto S, Liu J, Dijkhuizen L, Eltis LD. 2008. The actinobacterial mce4 locus encodes a steroid transporter. J Biol Chem 283:35368–35374. https://doi.org/10.1074/jbc.M805496200
78. Sutcliffe IC, Brown AK, Dover LG. 2010. The *Rhodococcal* cell envelope: composition, organisation and biosynthesis, p 29–71. In Alvarez HM (ed), Biology of *Rhodococcus*. Microbiology monographs. Springer, Berlin, Heidelberg. https://doi.org/10.1007/978-3-642-12937-7
79. de Carvalho C. 2019. Adaptation of *Rhodococcus* to organic solvents, p 103–135. In Alvarez H (ed), Biology of *Rhodococcus*. Microbiology monographs. Springer, Cham. https://doi.org/10.1007/978-3-030-11461-9
80. Eberlein C, Baumgarten T, Starke S, Heipieper HJ. 2018. Immediate response mechanisms of gram-negative solvent-tolerant bacteria to cope with environmental stress: cis-trans isomerization of unsaturated fatty acids and outer membrane vesicle secretion. Appl Microbiol Biotechnol 102:2583–2593. https://doi.org/10.1007/s00253-018-8832-9
81. de Carvalho C. 2012. Adaptation of *Rhodococcus erythropolis* cells for growth and bioremediation under extreme conditions. Res Microbiol 163:125–136. https://doi.org/10.1016/j.resmic.2011.11.003
82. Chen S, Zang M, Li L, Chen J, Liu Q, Feng X, Sun S, Zang C, Zhao C. 2021. Efficient biodesulfurization of diesel oil by *Gordonia* sp. SC-10 with highly hydrophobic cell surfaces. Biochem Eng J 174:108094. https://doi.org/10.1016/j.bej.2021.108094
83. de Carvalho C, Wick LY, Heipieper HJ. 2009. Cell wall adaptations of planktonic and biofilm *Rhodococcus erythropolis* cells to growth on C5 to C16 n-alkane hydrocarbons. Appl Microbiol Biotechnol 82:311–320. https://doi.org/10.1007/s00253-008-1809-3
84. Xu X-Q, Beardall J. 1997. Effect of salinity on fatty acid composition of a green microalga from an antarctic hypersaline lake. Phytochemistry 45:655–658. https://doi.org/10.1016/S0031-9422(96)00868-0
85. Presentato A, Cappelletti M, Sansone A, Ferreri C, Piacenza E, Demeter MA, Crognale S, Petruccioli M, Milazzo G, Fedi S, Steinbüchel A, Turner RJ, Zannoni D. 2018. Aerobic growth of *Rhodococcus aetherivorans* BCP1 using selected naphthenic acids as the sole carbon and energy sources. Front Microbiol 9:672. https://doi.org/10.3389/fmicb.2018.00672
86. Watanabe K, Noda K, Maruhashi K. 2003. Enhanced desulfurization in a transposon-mutant strain of *Rhodococcus erythropolis*. Biotechnol Lett 25:1299–1304. https://doi.org/10.1023/a:1024943121138
87. Kondakova T, D'Heygère F, Feuilloley MJ, Orange N, Heipieper HJ, Duclairoir Poc C. 2015. Glycerophospholipid synthesis and functions in *Pseudomonas*. Chem Phys Lipids 190:27–42. https://doi.org/10.1016/j.chemphyslip.2015.06.006
88. Kaval KG, Garsin DA. 2018. Ethanolamine utilization in bacteria. mBio 9:e00066-18. https://doi.org/10.1128/mBio.00066-18
89. Burg MB, Ferraris JD. 2008. Intracellular organic osmolytes: function and regulation. J Biol Chem 283:7309–7313. https://doi.org/10.1074/jbc.R700042200
90. Dávila Costa JS, Herrero OM, Alvarez HM, Leichert L. 2015. Label-free and redox proteomic analyses of the triacylglycerol-accumulating *Rhodococcus Jostii* RHA1. Microbiology (Reading) 161:593–610. https://doi.org/10.1099/mic.0.000028
91. Munyati-Othman N, Appasamy SD, Damiri N, Emrizal R, Alipiah NM, Ramlan EI, Firdaus-Raih M. 2021. Regulation of glycine cleavage and detoxification by a highly conserved glycine riboswitch in *Burkholderia* spp. Curr Microbiol 78:2943–2955. https://doi.org/10.1007/s00284-021-02550-5
92. Li S, Ma T. 2019. The desulfurization pathway in *Rhodococus*, p 203–229. In Alvarez H (ed), Biology of *Rhodococcus*. Microbiology monographs. Springer, Cham. https://doi.org/10.1007/978-3-030-11461-9
93. Tezuka T, Ohnishi Y. 2014. Two glycine riboswitches activate the glycine cleavage system essential for glycine detoxification in *Streptomyces griseus*. J Bacteriol 196:1369–1376. https://doi.org/10.1128/JB.01480-13
94. Holmqvist E, Wagner EGH. 2017. Impact of bacterial sRNAs in stress responses. Biochem Soc Trans 45:1203–1212. https://doi.org/10.1042/BST20160363
95. Apura P, de Lorenzo V, Arraiano CM, Martínez-García E, Viegas SC. 2021. Ribonucleases control distinct traits of *Pseudomonas putida* lifestyle. Environ Microbiol 23:174–189. https://doi.org/10.1111/1462-2920.15291
96. Zahrt TC, Deretic V. 2001. *Mycobacterium tuberculosis* signal transduction system required for persistent infections. Proc Natl Acad Sci U S A 98:12706–12711. https://doi.org/10.1073/pnas.221272198
97. He H, Hovey R, Kane J, Singh V, Zahrt TC. 2006. MprAB is a stress-responsive two-component system that directly regulates expression of sigma factors SigB and SigE in *Mycobacterium tuberculosis*. J Bacteriol 188:2134–2143. https://doi.org/10.1128/JB.188.6.2134-2143.2006
98. Su X, Guo L, Ding L, Qu K, Shen C. 2016. Induction of viable but nonculturable state in *Rhodococcus* and transcriptome analysis using RNA-seq. PLoS One 11:e0147593. https://doi.org/10.1371/journal.pone.0147593
99. Sibanda T, Buys EM. 2022. *Listeria monocytogenes* pathogenesis: the role of stress adaptation. Microorganisms 10:1522. https://doi.org/10.3390/microorganisms10081522
100. Singh RK, Jaiswal LK, Nayak T, Rawat RS, Kumar S, Rai SN, Gupta A. 2022. Expression, purification, and *in silico* characterization of *Mycobacterium smegmatis* alternative sigma factor SigB. Dis Markers 2022:7475704. https://doi.org/10.1155/2022/7475704
101. Jürgenstein K, Tagel M, Ilves H, Leppik M, Kivisaar M, Remme J. 2022. Variance in translational fidelity of different bacterial species is affected by pseudouridines in the tRNA anticodon stem-loop. RNA Biol 19:1050–1058. https://doi.org/10.1080/15476286.2022.2121447
102. Pollo-Oliveira L, Davis NK, Hossain I, Ho P, Yuan Y, Salguero García P, Pereira C, Byrne SR, Leng J, Sze M, Blaby-Haas CE, Sekowska A, Montoya A, Begley T, Danchin A, Aalberts DP, Angerhofer A, Hunt J, Conesa A, Dedon PC, de Crécy-Lagard V. 2022. The absence of the queuosine tRNA modification leads to pleiotropic phenotypes revealing perturbations of metal and oxidative stress homeostasis in *Escherichia coli* K12. Metallomics 14:mfac065. https://doi.org/10.1093/mtomcs/mfac065
103. Esberg B, Björk GR. 1995. The methylthio group (ms2) of N6-(4-hydroxyisopentenyl)-2-methylthioadenosine (ms2io6A) present next to the anticodon contributes to the decoding efficiency of the tRNA. J Bacteriol 177:1967–1975. https://doi.org/10.1128/jb.177.8.1967-1975.1995
104. Carpentier P, Leprêtre C, Basset C, Douki T, Torelli S, Duarte V, Hamdane D, Fontecave M, Atta M. 2020. Structural, biochemical and functional analyses of tRNA-monooxygenase enzyme MiaE from *Pseudomonas putida* provide insights into tRNA/MiaE interaction. Nucleic Acids Res 48:9918–9930. https://doi.org/10.1093/nar/gkaa667
105. Morais P, Adachi H, Yu Y-T. 2021. The critical contribution of pseudouridine to mRNA COVID-19 vaccines. Front Cell Dev Biol 9:789427. https://doi.org/10.3389/fcell.2021.789427
106. Noguchi S, Nishimura Y, Hirota Y, Nishimura S. 1982. Isolation and characterization of an *Escherichia coli* mutant lacking tRNA-guanine transglycosylase. Function and biosynthesis of queuosine in tRNA. J Biol Chem 257:6544–6550. https://doi.org/10.1016/S0021-9258(20)65176-6
107. Thibessard A, Borges F, Fernandez A, Gintz B, Decaris B, Leblond-Bourget N. 2004. Identification of *Streptococcus thermophilus* CNRZ368 genes involved in defense against superoxide stress. Appl Environ Microbiol 70:2220–2229. https://doi.org/10.1128/AEM.70.4.2220-2229.2004
108. Pal A, Iyer MS, Srinivasan S, Narain Seshasayee AS, Venkatesh KV. 2022. Global pleiotropic effects in adaptively evolved *Escherichia coli* lacking CRP reveal molecular mechanisms that define the growth physiology. Open Biol 12:210206. https://doi.org/10.1098/rsob.210206
109. Juarez A, Villa JA, Lanza VF, Lázaro B, de la Cruz F, Alvarez HM, Moncalián G. 2017. Nutrient starvation leading to triglyceride accumulation activates the Entner Doudoroff pathway in *Rhodococcus jostii* RHA1. Microb Cell Fact 16:35. https://doi.org/10.1186/s12934-017-0651-7
110. Grant CE, Bailey TL, Noble WS. 2011. FIMO: scanning for occurrences of a given motif. Bioinformatics 27:1017–1018. https://doi.org/10.1093/bioinformatics/btr064
111. Bailey TL, Johnson J, Grant CE, Noble WS. 2015. The MEME suite. Nucleic Acids Res 43:W39–W49. https://doi.org/10.1093/nar/gkv416

112. Percudani R, Peracchi A. 2009. The B6 database: a tool for the description and classification of vitamin B6-dependent enzymatic activities and of the corresponding protein families. BMC Bioinformatics 10:273. https://doi.org/10.1186/1471-2105-10-273
113. Tramonti A, Ghatge MS, Babor JT, Musayev FN, di Salvo ML, Barile A, Colotti G, Giorgi A, Paredes SD, Donkor AK, Al Mughram MH, de Crécy-Lagard V, Safo MK, Contestabile R. 2022. Characterization of the *Escherichia coli* pyridoxal 5'-phosphate homeostasis protein (YggS): role of lysine residues in PLP binding and protein stability. Protein Sci 31:e4471. https://doi.org/10.1002/pro.4471
114. Balabanova L, Averianova L, Marchenok M, Son O, Tekutyeva L. 2021. Microbial and genetic resources for cobalamin (vitamin B12) biosynthesis: from ecosystems to industrial biotechnology. Int J Mol Sci 22:4522. https://doi.org/10.3390/ijms22094522
115. Jousse C, Dalle C, Canet I, Lagrée M, Traïkia M, Lyan B, Mendes C, Sancelme M, Amato P, Delort A-M. 2017. Metabolomic study of the response to cold shock in a strain of *Pseudomonas syringae* isolated from cloud water. Metabolomics 14:11. https://doi.org/10.1007/s11306-017-1295-7
116. Cappelletti M, Presentato A, Piacenza E, Firrincieli A, Turner RJ, Zannoni D. 2020. Biotechnology of *Rhodococcus* for the production of valuable compounds. Appl Microbiol Biotechnol 104:8567–8594. https://doi.org/10.1007/s00253-020-10861-z
117. Veeranagouda Y, Lim EJ, Kim DW, Kim J-K, Cho K, Heipieper HJ, Lee K. 2009. Formation of specialized aerial architectures by *Rhodococcus* during utilization of vaporized p-cresol. Microbiology (Reading) 155:3788–3796. https://doi.org/10.1099/mic.0.029926-0
118. Alvarez HM, Steinbüchel A. 2019. Biology of triacylglycerol accumulation by *Rhodococcus*, p 299–332. In Alvarez H (ed), Biology of *Rhodococcus*. Microbiology monographs. Springer, Cham. https://doi.org/10.1007/978-3-030-11461-9
119. Baumgarten T, Sperling S, Seifert J, von Bergen M, Steiniger F, Wick LY, Heipieper HJ. 2012. Membrane vesicle formation as a multiple-stress response mechanism enhances *Pseudomonas putida* DOT-T1E cell surface hydrophobicity and biofilm formation. Appl Environ Microbiol 78:6217–6224. https://doi.org/10.1128/AEM.01525-12
120. Eberlein C, Starke S, Doncel ÁE, Scarabotti F, Heipieper HJ. 2019. Quantification of outer membrane vesicles: a potential tool to compare response in *Pseudomonas putida* KT2440 to stress caused by alkanols. Appl Microbiol Biotechnol 103:4193–4201. https://doi.org/10.1007/s00253-019-09812-0
121. Kuang S, Fan X, Peng R. 2018. Quantitative proteomic analysis of *Rhodococcus ruber* responsive to organic solvents. Biotechnol Biotechnol Equip 32:1418–1430. https://doi.org/10.1080/13102818.2018.1533432
122. Czech L, Hermann L, Stöveken N, Richter AA, Höppner A, Smits SHJ, Heider J, Bremer E. 2018. Role of the extremolytes ectoine and hydroxyectoine as stress protectants and nutrients: genetics, phylogenomics, biochemistry, and structural analysis. Genes (Basel) 9:177. https://doi.org/10.3390/genes9040177
123. Forquin M-P, Hébert A, Roux A, Aubert J, Proux C, Heilier J-F, Landaud S, Junot C, Bonnarme P, Martin-Verstraete I. 2011. Global regulation of the response to sulfur availability in the cheese-related bacterium *Brevibacterium aurantiacum*. Appl Environ Microbiol 77:1449–1459. https://doi.org/10.1128/AEM.01708-10
124. Groshong AM, Dey A, Bezsonova I, Caimano MJ, Radolf JD. 2017. Peptide uptake is essential for *Borrelia burgdorferi* viability and involves structural and regulatory complexity of its oligopeptide transporter. mBio 8:e02047-17. https://doi.org/10.1128/mBio.02047-17
125. Irving SE, Choudhury NR, Corrigan RM. 2021. The stringent response and physiological roles of (pp)pGpp in bacteria. Nat Rev Microbiol 19:256–271. https://doi.org/10.1038/s41579-020-00470-y